

CERN-EP-2021-233
7 November 2021

$K_S^0 K_S^0$ and $K_S^0 K^\pm$ femtoscopy in pp collisions at $\sqrt{s} = 5.02$ and 13 TeV

ALICE Collaboration*

Abstract

Femtoscopic correlations with the particle pair combinations $K_S^0 K_S^0$ and $K_S^0 K^\pm$ are studied in pp collisions at $\sqrt{s} = 5.02$ and 13 TeV by the ALICE experiment. At both energies, boson source parameters are extracted for both pair combinations, by fitting models based on Gaussian size distributions of the sources, to the measured two-particle correlation functions. The interaction model used for the $K_S^0 K_S^0$ analysis includes quantum statistics and strong final-state interactions through the $f_0(980)$ and $a_0(980)$ resonances. The model used for the $K_S^0 K^\pm$ analysis includes only the final-state interaction through the a_0 resonance. Source parameters extracted in the present work are compared with published values from pp collisions at $\sqrt{s} = 7$ TeV and the different pair combinations are found to be consistent. From the observation that the strength of the $K_S^0 K_S^0$ correlations is significantly greater than the strength of the $K_S^0 K^\pm$ correlations, the new results are compatible with the a_0 resonance being a tetraquark state of the form $(q_1, \bar{q}_2, s, \bar{s})$, where q_1 and q_2 are u or d quarks.

arXiv:2111.06611v2 [nucl-ex] 5 Dec 2022

© 2021 CERN for the benefit of the ALICE Collaboration.

Reproduction of this article or parts of it is allowed as specified in the CC-BY-4.0 license.

*See Appendix A for the list of collaboration members

1 Introduction

Identical boson femtoscopy, especially identical charged $\pi^\pm \pi^\pm$ femtoscopy, has been used extensively over the years to study experimentally the space-time geometry of the collision region in high-energy proton and heavy-ion collisions [1]. More recently, identical-kaon femtoscopy studies have been reported for a variety of colliding systems, energies and kaon pairs: $K_S^0 K_S^0$ pairs in Au–Au collisions at $\sqrt{s_{NN}} = 0.2$ TeV by the STAR collaboration [2], $K_S^0 K_S^0$ and $K^\pm K^\pm$ pairs in pp collisions at $\sqrt{s} = 7$ TeV and Pb–Pb collisions at $\sqrt{s_{NN}} = 2.76$ TeV by the ALICE collaboration [3–5]. Identical-kaon femtoscopy gives information about the collision region that is complementary to that obtained in identical-pion femtoscopy in that it probes the hotter region where strange quarks are produced and extends the momentum range over which the femtoscopy analysis can be applied. Also, the kaon analyses are expected to offer a cleaner signal compared to pions, as they are less affected by resonance decays.

Non-identical kaon femtoscopy with $K_S^0 K^\pm$ pairs was first measured by ALICE in pp collisions at $\sqrt{s} = 7$ TeV and Pb–Pb collisions at $\sqrt{s_{NN}} = 2.76$ TeV [6, 7]. Although the space-time geometry of the kaon source can be extracted with these pairs, the main emphasis of non-identical kaon femtoscopy is to obtain information about the strong final-state interaction (FSI) between the kaons. For the identical kaon cases the interactions are, for $K^\pm K^\pm$: quantum statistics, Coulomb interaction, and for $K_S^0 K_S^0$: quantum statistics, FSI through $f_0(980)$ and $a_0(980)$ threshold resonances [2]. For the $K_S^0 K^\pm$, the only FSI is through the a_0 resonance. Note that “threshold resonances”, like the a_0 and f_0 , are resonances where the sum of the masses of the decay particles is very close in value to the mass of the resonance. A non-resonant FSI in the $K_S^0 K_S^0$ pair is expected to be small compared with the resonant f_0 and a_0 FSI and can be neglected to first order [2, 8]. The only pair-wise interaction expected for a $K_S^0 K^\pm$ pair at freeze out from the collision system is a FSI through the a_0 resonance. This is because there is no quantum statistics enhancement for non-identical kaons, no Coulomb effect since one of the kaons is neutral, and no strong FSI through the f_0 resonance since the kaon pair is in an isospin-1 state, as is the a_0 , whereas the f_0 is isospin-0 and thus isospin would not be conserved.

Another feature of the $K_S^0 K^\pm$ FSI through the a_0 resonance is that since the a_0 has zero strangeness, and the K_S^0 is composed of a linear combination of the K^0 and \bar{K}^0 , only the $\bar{K}^0 K^+$ pair from $K_S^0 K^+$ and the $K^0 K^-$ pair from $K_S^0 K^-$ can form a_0 resonances in order to conserve zero strangeness. This feature allows the K^0 and \bar{K}^0 sources to be studied separately. However, it was concluded in the previous ALICE $K_S^0 K^\pm$ publications that there is no significant difference in the source parameters between $K_S^0 K^+$ and $K_S^0 K^-$ [6, 7].

Lastly, the $K_S^0 K^\pm$ FSI allows the properties of the a_0 resonance itself to be studied. This is interesting in its own right since many works exist in the literature discussing the possibility that the a_0 could be a 4-quark state, i.e. a tetraquark. It was first suggested in 1977 that experimentally-observed low-lying mesons, such as the a_0 , are part of a SU(3) tetraquark nonet using a quark model [9]. A later follow-up calculation was published reinforcing this work using lattice QCD calculations [10]. Since then, there have been a number of QCD studies of these mesons that fall in the categories of QCD-inspired models, for example Refs. [11–14], and lattice QCD calculations, for example Refs. [15–17]. An interesting result that was found from the previous measurements in comparing the strengths, i.e. λ -parameters, of the $K_S^0 K_S^0$ and $K_S^0 K^\pm$ correlations with each other was that the strength of the $K_S^0 K_S^0$ correlations is significantly larger than the strength of the $K_S^0 K^\pm$ correlations measured in $\sqrt{s} = 7$ TeV pp collisions. It was suggested that this could be an indication that the a_0 is a tetraquark state [6, 7].

In light of the interesting results from the $\sqrt{s} = 7$ TeV pp measurements, the main motivations to extend the measurements to $\sqrt{s} = 5.02$ and 13 TeV pp collisions are the following:

- In these new measurements, we investigate the collision-energy dependence of the λ difference between $K_S^0 K_S^0$ and $K_S^0 K^\pm$. A lack of a dependence on the center-of-mass energy would be consistent

with the tetraquark interpretation of the $a_0(980)$.

- The previous paper compared results for λ that were obtained and published seven years apart, i.e. $K_S^0 K_S^0$ in PLB from 2012 [3] and $K_S^0 K^\pm$ in PLB from 2019 [6], and that were analyzed in different ways. The $K_S^0 K_S^0$ analysis from the 2012 paper was done in several multiplicity ranges which had to be averaged in order to compare with the minimum-bias 2019 $K_S^0 K^\pm$ result. However, in the present paper the new $K_S^0 K_S^0$ and $K_S^0 K^\pm$ analyses were done at the same time and using the same kinematic ranges. By carrying out simultaneous measurements of $K_S^0 K_S^0$ and $K_S^0 K^\pm$ this results in a better comparison with each other.
- In this new analysis a detailed calculation of the effect of long-lived resonances on the λ parameter is presented to better establish that this contamination is not responsible for the λ difference.

2 Description of experiment and data selection

Data taken by the ALICE experiment [18] in the LHC Run 2 period (2015–2018) were employed in the present analysis. This analysis used both $\sqrt{s} = 5.02$ TeV and 13 TeV reconstructed minimum bias triggered pp collisions, giving about 0.5×10^9 and 1.5×10^9 events, respectively. Monte Carlo (MC) simulations were used for determining selection values, momentum resolution and purity studies, and for the baseline underlying the signal for the case of the $K_S^0 K_S^0$ analyses. In the MC calculations, particles from pp collision events simulated by the general-purpose generator PYTHIA8 [19] with the Monash 2013 tune [20] were transported through a GEANT3 [21] model of the ALICE detector. The total numbers of MC events used in the $\sqrt{s} = 5.02$ and 13 TeV analyses were about 0.7×10^9 and 1.2×10^9 , respectively.

The V0 detectors, which consist of two arrays of scintillators located along the beamline and covering the full azimuth [22, 23] were used for triggering and event selection. Charged particles were reconstructed and identified with the central barrel detectors located within a solenoid magnet with a field strength of magnitude $B = 0.5$ T. Charged particle tracking was performed using the Time Projection Chamber (TPC) [24] and the Inner Tracking System (ITS) [18]. The momentum determination for K^\pm was made using only the TPC. The ITS allowed for high spatial resolution in determining the primary collision vertex, which was used to constrain the TPC tracks. An average momentum resolution of less than 10 MeV/c was typically obtained for the charged tracks of interest in this analysis [25]. The primary vertex was obtained from the ITS, the position being constrained along the beam direction to be within ± 10 cm of the center of the ALICE detector. In addition to the standard track quality selections [25], the selections based on the quality of track fitting and the number of detected tracking points in the TPC were used to ensure that only well-reconstructed tracks were taken into account in the analysis [24–26].

Particle Identification (PID) for reconstructed tracks was carried out using both the TPC and the Time-Of-Flight (TOF) detectors in the pseudorapidity range $|\eta| < 0.8$ [26, 27]. For the PID signal from both detectors, a value (N_σ) was assigned to each track denoting the number of standard deviations between the measured track information and expected values, assuming a mass hypothesis, divided by the detector resolution [5, 25–27]. For TPC PID, a parametrized Bethe-Bloch formula was used to calculate the specific energy loss $\langle dE/dx \rangle$ in the detector expected for a particle with a given charge, mass and momentum. For PID with TOF, the particle mass was used to calculate the expected time-of-flight as a function of track length and momentum.

Other event selection criteria were also applied. The event must have one accepted possible $K_S^0 K_S^0$ or $K_S^0 K^\pm$ pair. Pile-up events were rejected using the standard ALICE pile-up rejection method [26]. Pile-up effects were also investigated by performing the analysis using only low-luminosity data-taking periods. No significant difference was found in the extracted R and λ parameters compared with the higher count-rate runs used.

Table 1: Single-particle selection criteria.

Neutral kaon selection	Value
Daughter p_T	$> 0.15 \text{ GeV}/c$
Daughter $ \eta $	< 0.8
Daughter DCA (3D) to primary vertex	$> 0.4 \text{ cm}$
Daughter TPC N_σ	< 3
Daughter TOF N_σ (for $p > 0.8 \text{ GeV}/c$)	< 3
$ \eta $	< 0.8
DCA (3D) π^+ to π^-	$< 0.3 \text{ cm}$
DCA (3D) of K_S^0 to primary vertex	$< 0.3 \text{ cm}$
Decay length (3D, lab frame)	$< 30 \text{ cm}$
Decay radius (2D, lab frame)	$> 0.2 \text{ cm}$
Cosine of pointing angle	> 0.99
Invariant mass	$0.485 < m < 0.510 \text{ GeV}/c^2$
Charged kaon selection	Value
p_T	$0.15 < p_T < 1.2 \text{ GeV}/c$
$ \eta $	< 0.8
Transverse DCA to primary vertex	$< 2.4 \text{ cm}$
Longitudinal DCA to primary vertex	$< 3.0 \text{ cm}$
N_σ^{TOF} with valid TOF signal and $p > 0.5 \text{ GeV}/c$	< 2
N_σ^{TPC} if no TOF signal for all p_T	< 2
Kalman fit χ^2/N^{clus}	≤ 4

2.1 Kaon selection

The methods used to select and identify individual K_S^0 and K^\pm particles are the same as those used for the ALICE $K_S^0 K_S^0$ [3] and $K^\pm K^\pm$ [4] analyses in pp collisions at $\sqrt{s} = 7 \text{ TeV}$, and are described in the following sections.

2.1.1 K_S^0 reconstruction

Using an invariant mass technique, the neutral K_S^0 vertices and parameters are reconstructed and calculated from pairs of detected $\pi^+ \pi^-$ tracks. Single-particle selection criteria for the K_S^0 and the pions, for example particle momentum (p), transverse momentum (p_T), and pseudorapidity (η), are shown in Table 1.

Most of the topological selection criteria ($\pi^+ \pi^-$ distance-of-closest-approach (DCA), π -vertex DCA, K_S^0 DCA, and decay length) were chosen to optimize purity and statistical significance. If two reconstructed K_S^0 particles share a daughter track, both are removed from the analysis. The selection criteria in this analysis are comparable to or stricter than those in other K_S^0 analyses; strict selection criteria are favored to increase the sample purity.

A candidate K_S^0 vertex with a reconstructed invariant mass within $0.485 < m(\pi^+ \pi^-) < 0.510 \text{ GeV}/c^2$ is identified as a K_S^0 . In this range, the single- K_S^0 purity is measured to be $98 \pm 1\%$ for the k_T interval of $0.5 < k_T < 0.7 \text{ GeV}/c$, where $k_T = |\vec{p}_{T1} + \vec{p}_{T2}|/2$, and where \vec{p}_{T1} and \vec{p}_{T2} are the transverse momenta of the particles in the pair. The purity here is defined as $\text{Signal}/(\text{Signal} + \text{Background})$ and is calculated by fitting a fourth-order polynomial to the background in the combined invariant mass intervals $0.4\text{--}0.45 \text{ GeV}/c^2$ and $0.55\text{--}0.6 \text{ GeV}/c^2$ and using the bin contents of the invariant mass histogram as the ‘‘Signal + Background’’. No selection on p_T is employed in this analysis for K_S^0 . Having a pair purity less than unity will be reflected in the lowering of the λ parameter, which can later be corrected for purity, however the K_S^0 purity is very close to unity for this analysis.

2.1.2 K^\pm identification

As mentioned above, charged kaons are selected using the TPC and TOF detectors with the same methods as employed in Refs. [4, 5]. The quality of the track is determined by the χ^2/N^{clus} value for the Kalman fit to the reconstructed position of the TPC clusters (N^{clus} is the number of clusters attached to the track). The track is rejected if the value is larger than 4.0. The selection criteria used for the charged kaon selection in the TPC and TOF are shown in Table 1. In the table, N_σ^{TPC} and N_σ^{TOF} are the numbers of standard deviations the TPC energy-loss and TOF signal are away from their predicted values divided by detector resolution, respectively.

The average charged kaon purity is found using PYTHIA8 MC simulations to be $91 \pm 1\%$ in the k_T range used in this analysis, i.e. $0.5 < k_T < 0.7$ GeV/ c . This is in agreement with the charged kaon purity found by the ALICE collaboration in Ref. [5].

2.2 Two-track selection

Experimental two-track effects, such as the merging of two real tracks into one reconstructed track and the splitting of one real track into two reconstructed tracks, is a challenge for femtoscopic studies. These effects are observed for tracks with small average separation in the TPC. For each pair of like-sign tracks, which could be pions from two K_S^0 decays, or the pion from a K_S^0 decay and the same-charged K^\pm track, the distance between the tracks was calculated at up to nine positions throughout the TPC (every 20 cm along the radial direction from 85 cm to 245 cm) and then averaged. When comparing the distribution of the average separation of track pairs from single events with the distribution from pairs constructed of tracks from different events (mixed events), a splitting enhancement is seen in the same-events for average separations approaching zero. For the distribution of mixed-event tracks, the primary vertex position for each track was subtracted from each track point to mock them up as coming from the same event. To minimize this splitting effect, this analysis demanded that the tracks must have an average TPC separation of at least 13 cm.

3 Two-particle correlation function

This analysis studies the momentum correlations of $K_S^0 K_S^0$ and $K_S^0 K^\pm$ pairs using the two-particle correlation function, defined as $C(k^*) = A(k^*)/B(k^*)$, where $A(k^*)$ is the measured distribution of real pairs from the same event and $B(k^*)$ is the reference distribution of pairs from mixed events. The quantity k^* is the momentum of one of the particles in the pair rest frame, and for the general case of two particles with unequal mass, m_1 and m_2 , is given by

$$k^* = \sqrt{\frac{w^2 - m_1^2 m_2^2}{2w + m_1^2 + m_2^2}} \quad (1)$$

where,

$$w \equiv (q_{\text{inv}}^2 + m_1^2 + m_2^2)/2. \quad (2)$$

The square of the invariant momentum difference $q_{\text{inv}}^2 = |\vec{p}_1 - \vec{p}_2|^2 - |E_1 - E_2|^2$ is most conveniently evaluated with the momenta and energies of the two particles measured in the lab frame. Note that $m_1 = m_2$ gives $k^* = q_{\text{inv}}/2$. The denominator $B(k^*)$ is formed by mixing particles from each event with particles from ten other events in the same z -vertex bin (2 cm width) and of similar event multiplicity. A k^* bin size of 20 MeV/ c was used in all cases.

As mentioned earlier, correlation functions are calculated for minimum bias events and a k_T range from 0.5–0.7 GeV/ c . This closely reproduces the conditions for the kaon femtoscopy measurements with $K_S^0 K_S^0$ and $K_S^0 K^\pm$ pairs published by ALICE for pp collisions at $\sqrt{s} = 7$ TeV with which the present

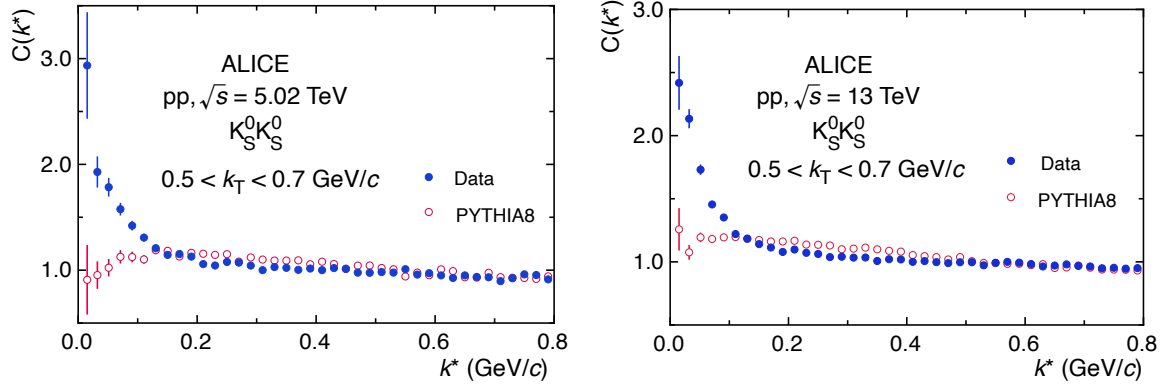


Figure 1: Example $K_S^0 K_S^0$ correlation functions along with the resulting distributions from PYTHIA8 simulations in pp collisions at $\sqrt{s} = 5.02$ (left) and 13 TeV (right).

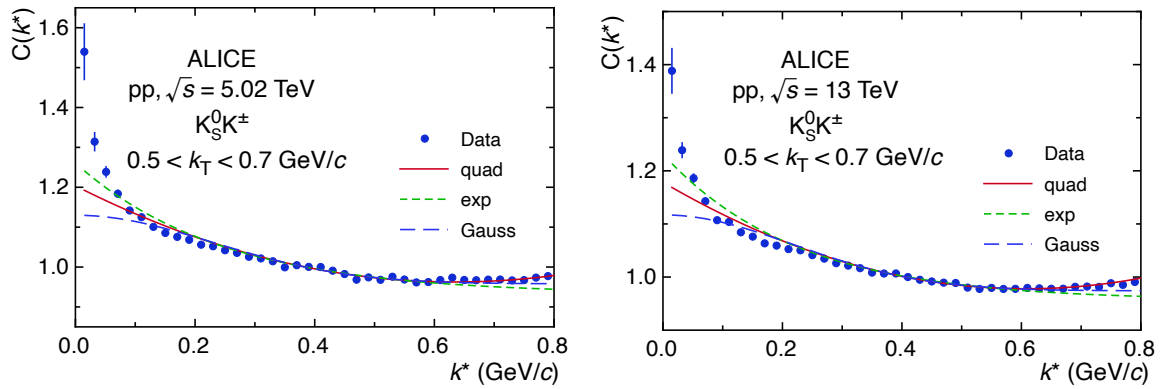


Figure 2: Example $K_S^0 K^\pm$ correlation functions plotted with fits of Eqs. 3, 4 and 5 in pp collisions at $\sqrt{s} = 5.02$ (left) and 13 TeV (right).

results will be compared [3, 6]. The k_T range used encompasses the peak in the k_T distributions at each collision energy. Also, the pseudorapidity density of charged particles at midrapidity, $dN_{ch}/d\eta$, is found to be small in pp collisions and has a weak dependence on \sqrt{s} , measured to be 5.91 ± 0.45 , $6.01^{+0.20}_{-0.12}$, and 7.60 ± 0.50 for $\sqrt{s} = 5.02, 7$ and 13 TeV, respectively, where the uncertainties are the statistical and systematic uncertainties added in quadrature [28–30].

Figure 1 shows an example of raw experimental $K_S^0 K_S^0$ correlation functions along with the resulting distributions from PYTHIA8 simulations normalized in the k^* region 0.6–0.8 GeV/c for $\sqrt{s} = 5.02$ and 13 TeV. Note that the PYTHIA8 calculations do not contain FSI or femtosopic correlations. Figure 2 shows an example of raw experimental $K_S^0 K^\pm$ correlation functions plotted with baseline fits for various functions (see below) for $\sqrt{s} = 5.02$ and 13 TeV. The raw correlation functions from the data are enhanced for $k^* < 0.1$ GeV/c due to quantum statistics and the FSI of the f_0 and a_0 and slightly suppressed in the region $0.1 < k^* < 0.4$ GeV/c due to the FSI for $K_S^0 K_S^0$. For $K_S^0 K^\pm$ the FSI of the a_0 produces similar but smaller enhancements and suppressions in the same general k^* regions. For $k^* > 0.4$ GeV/c a non-flat baseline is observed in both cases. PYTHIA8 fairly describes the non-flat baseline of the experimental correlation functions for $K_S^0 K_S^0$, and is thus used to take out the effect of the non-flat baseline by dividing the raw experimental correlation functions by the PYTHIA8 correlation functions in those cases. This is a similar method as was used for the $\sqrt{s} = 7$ TeV pp $K_S^0 K_S^0$ measurements [3].

Unlike the case for $K_S^0 K_S^0$, which has a relatively large signal compared with the baseline, for the $K_S^0 K^\pm$ correlation functions PYTHIA8 is not sensitive enough to model the baseline sufficiently well with respect to the significantly smaller enhancement and suppression produced by the FSI of the a_0 alone.

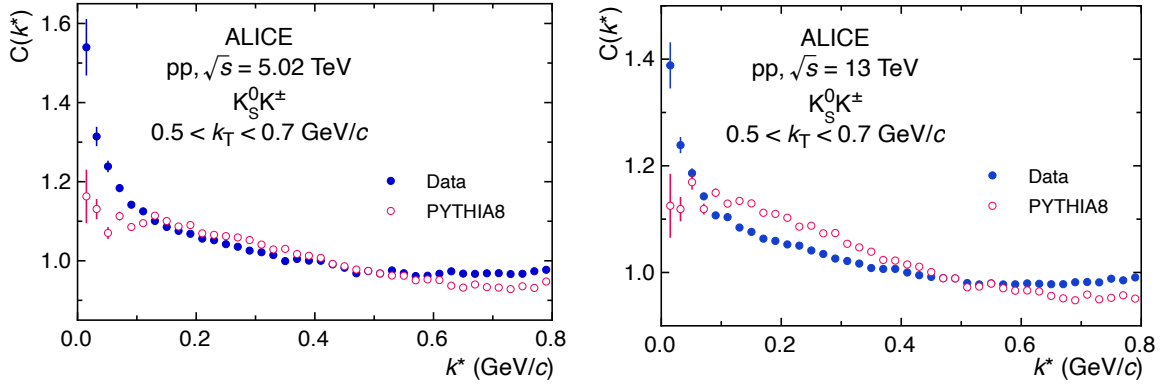


Figure 3: Example $K_S^0 K_S^\pm$ correlation functions along with the resulting distributions from PYTHIA8 simulations in pp collisions at $\sqrt{s} = 5.02$ (left) and 13 TeV (right).

Examples of this are shown in Fig. 3, which compares the raw $\sqrt{s} = 5.02$ and 13 TeV pp correlation functions from data with those from PYTHIA8. For these correlation functions, quadratic, exponential and Gaussian functions are used to model the baseline, as was done in Ref. [6] for the measurement in pp collisions at $\sqrt{s} = 7$ TeV, of the forms

$$C_{\text{quadratic}}(k^*) = a(1 - bk^* + ck^{*2}) \quad (3)$$

$$C_{\text{exponential}}(k^*) = a(1 + b \exp(-ck^*)) \quad (4)$$

$$C_{\text{Gaussian}}(k^*) = a(1 + b \exp(-ck^{*2})) \quad (5)$$

where a , b and c are parameters that are fitted to the experimental $C(k^*)$ simultaneously with the FSI model (see Section 4). As shown in Fig. 2, the quadratic, Gaussian and exponential functions all describe the data well in the k^* range of ~ 0.3 – 0.6 GeV/ c .

4 Fitting the correlation functions to extract the source parameters

4.1 $K_S^0 K_S^0$

The $K_S^0 K_S^0$ correlation functions were fitted with the Lednický parameterization [2] which incorporates quantum statistics with strong FSI. FSI arise in the $K_S^0 K_S^0$ channels due to the near-threshold resonances, $a_0(980)$ and $f_0(980)$. This parameterization is based on the model by R. Lednický and V.L. Lyuboshitz [31, 32].

The general form of the fit function is:

$$C_{\text{Lednický}}(k^*) = 1 + \lambda e^{-4k^{*2}R^2} + \lambda \alpha \left[\left| \frac{f(k^*)}{R} \right|^2 + \frac{4\mathcal{R}f(k^*)}{\sqrt{\pi}R} F_1(2k^*R) - \frac{2\mathcal{I}f(k^*)}{R} F_2(2k^*R) + \Delta C \right] \quad (6)$$

where

$$F_1(z) = \int_0^z dx \frac{e^{x^2 - z^2}}{z}; \quad F_2(z) = \frac{1 - e^{-z^2}}{z}. \quad (7)$$

Table 2: The f_0 and a_0 masses and coupling parameters used in the present analysis, all in GeV.

m_{f_0}	$\gamma_{f_0 K\bar{K}}$	$\gamma_{f_0 \pi\pi}$	m_{a_0}	$\gamma_{a_0 K\bar{K}}$	$\gamma_{a_0 \pi\eta}$
0.967	0.34	0.089	1.003	0.8365	0.4580

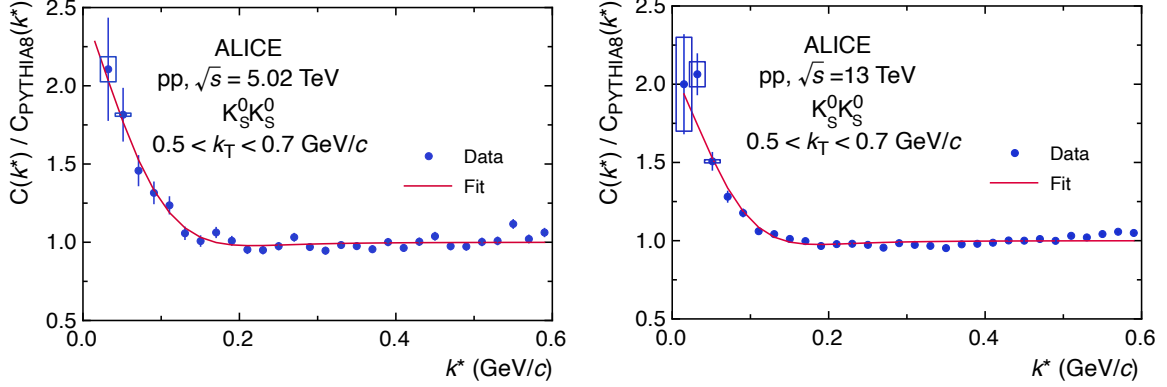


Figure 4: Example fits of Eq. 6 to the ratio of the data to PYTHIA8 correlation functions for $K_S^0 K_S^0$ in pp collisions at $\sqrt{s} = 5.02$ TeV (left) and 13 TeV (right). Statistical uncertainties are shown as error bars and systematic uncertainties are shown as boxes.

The scattering amplitude is

$$f(k^*) = \frac{f_0(k^*) + f_1(k^*)}{2} \quad (8)$$

where

$$f_1(k^*) = \frac{\gamma_1}{m_1^2 - s - i(\gamma_1 k^* + \gamma_1' k_1')}, \quad (9)$$

$f(k^*)$ is the s-wave $K^0 \bar{K}^0$ scattering amplitude whose contributions are the isoscalar f_0 and isovector a_0 resonances; α is set to 0.5 assuming symmetry in K^0 and \bar{K}^0 production; R is the radius parameter; and λ is the correlation strength. In Eq. 9, $I=0$ or 1 for the f_0 or a_0 , m_1 is the mass of the resonance, and γ_1 and γ_1' are the couplings of the resonances to their decay channels. Also, $s = 4(m_K^2 + k^{*2})$ and k_1' denotes the momentum in the second decay channel. The $K^0 \bar{K}^0$ s-wave scattering amplitude depends on the f_0 and a_0 resonance mass and decay couplings, which have been measured [33]. The parameter set used in the present analysis is shown in Table 2. The quantity ΔC is a correction for small source sizes found in pp collisions [2], and is given by:

$$\Delta C = \frac{1}{\sqrt{\pi}R^3} \left[|f_0(k^*)|^2 \left(\frac{3}{\gamma_0} + \frac{1}{\gamma_1} \right) + |f_1(k^*)|^2 \left(\frac{1}{\gamma_0} + \frac{3}{\gamma_1} \right) \right]. \quad (10)$$

Figure 4 shows example fits of Eq. 6 to the ratio of the data to PYTHIA8 correlation functions for $K_S^0 K_S^0$ measured in pp collisions at $\sqrt{s} = 5.02$ TeV and 13 TeV. Statistical uncertainties are shown as error bars, and systematic uncertainties are shown as boxes. The statistical uncertainties from PYTHIA8 were propagated to those on the data points. The fits of Eq. 6 to the correlation function ratios provide a good description of the data, typically giving χ^2/ndf values close to unity. The χ^2/ndf values of the fits to the $K_S^0 K_S^0$ correlation functions are 1.3 and 2.5, respectively, for the left and the right figures. The large χ^2/ndf value for the fit shown in the right figure mostly reflects a combination of the small statistical uncertainties in the data and the deviation of the fit in the region $k^* > 0.5$ GeV/c.

4.2 $K_S^0 K^\pm$

The $K_S^0 K^\pm$ correlation functions were fitted with the expression:

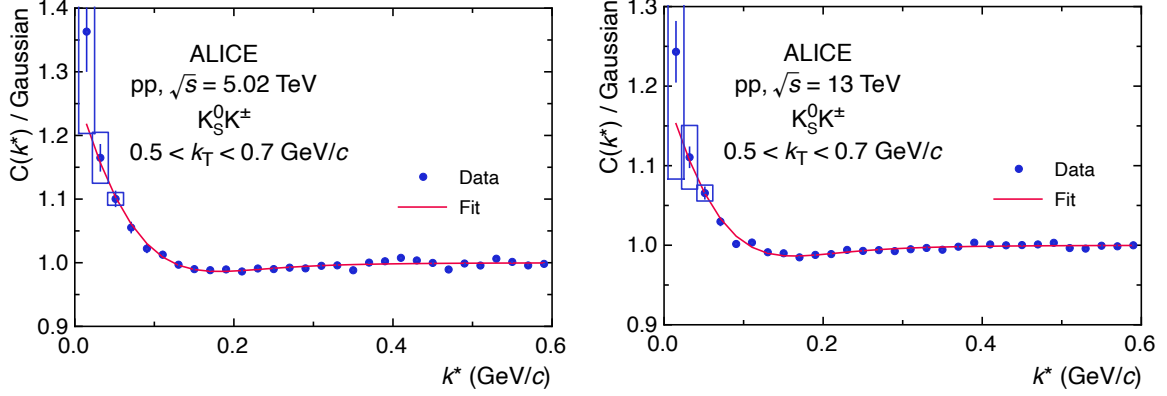


Figure 5: Example fits using Eq. 11 to the ratio of the data in pp collisions at $\sqrt{s} = 5.02$ TeV (left) and 13 TeV (right) to Eq. 5. Statistical uncertainties are shown as error bars and systematic uncertainties are shown as boxes.

$$C(k^*) = C_{\text{Lednicky2}}(k^*) C_{\text{baseline}}(k^*) \quad (11)$$

where $C_{\text{Lednicky2}}(k^*)$ is a modified version of Eq. 6, and $C_{\text{baseline}}(k^*)$ is Eq. 3, Eq. 4 or Eq. 5.

The modified form of the Lednický FSI fit function used is:

$$C_{\text{Lednicky2}}(k^*) = 1 + \left(\frac{\lambda \alpha}{2} \right) \left[\left| \frac{f(k^*)}{R} \right|^2 + \frac{4\mathcal{R}f(k^*)}{\sqrt{\pi}R} F_1(2k^*R) - \frac{2\mathcal{I}f(k^*)}{R} F_2(2k^*R) + \Delta C' \right]. \quad (12)$$

The scattering amplitude is:

$$f(k^*) = \frac{\gamma_{a_0 \rightarrow K\bar{K}}}{m_{a_0}^2 - s - i(\gamma_{a_0 \rightarrow K\bar{K}} k^* + \gamma_{a_0 \rightarrow \pi\eta} k_{\pi\eta})}. \quad (13)$$

Note that the form of the FSI term in Eq. 12 differs from the form of the FSI term for $K_S^0 K_S^0$ correlations, Eq. 6, by a factor of 1/2 due to the non-identical particles in $K_S^0 K^\pm$ correlations and thus the absence of the requirement to symmetrize the wavefunction. The $K^0 K^-$ or $\bar{K}^0 K^+$ s-wave scattering amplitude depends only on the a_0 resonance mass and decay couplings. The ones used in this analysis are shown in Table 2. The correction due to small source sizes, $\Delta C'$, now becomes:

$$\Delta C' = \frac{2}{\sqrt{\pi}R^3} \frac{|f(k^*)|^2}{\gamma_{a_0 \rightarrow K\bar{K}}}. \quad (14)$$

The fitting strategy is to make a 5-parameter fit of Eq. 11 to the $K_S^0 K^\pm$ experimental correlation functions to extract R , λ , a , b and c for each baseline functional form.

Figure 5 shows examples of correlation functions divided by the Gaussian baseline function, Eq. 5, with fits of Eq. 11 for $K_S^0 K^\pm$, i.e. summed over $K_S^0 K^+$ and $K_S^0 K^-$. The a_0 FSI parameterization coupled with the Gaussian baseline assumption is seen to give a good representation of the signal region of the data, i.e. reproducing the enhancement in the k^* region 0.0–0.1 GeV/c and the small dip in the region 0.1–0.3 GeV/c. The average χ^2/ndf for these fits to the correlation functions are 1.04 for the left figure and 1.13 for the right figure. Fits to the data with similarly good χ^2/ndf values are also found using the exponential and quadratic baselines.

4.3 Systematic uncertainties

Table 3 shows the total systematic uncertainties of the extracted R and λ parameters from the $K_S^0 K_S^0$ and $K_S^0 K^\pm$ analyses. The total systematic uncertainty is generally higher than the statistical one. The total systematic uncertainty is taken as the square-root of the quadratic sum of the systematic uncertainty from the fit and the selection criteria.

The fit systematic uncertainty is the combined systematic uncertainty due to the various baseline assumptions and varying the k^* fit range. For $K_S^0 K_S^0$, it is calculated from the standard deviation of the extracted source parameters from six k^* fit ranges: 0.0–0.3, 0.0–0.4, 0.0–0.5, 0.0–0.6, 0.0–0.7 and 0.0–0.8 GeV/ c . For $K_S^0 K^\pm$ it is calculated from the standard deviation of using the three baseline functions in four k^* fit ranges: 0.0–0.3, 0.0–0.4, 0.0–0.5 and 0.0–0.6 GeV/ c . The fit values shown in Table 3 are the average values over these k^* ranges.

The selection systematic uncertainty is the systematic uncertainty related to the various selection criteria applied in the data analysis. To determine this, single particle selection criteria were varied by $\sim \pm 10\%$, and the value chosen for the minimum separation distance of like charge-sign tracks was varied by $\sim 20\%$. The uncertainties in the purity corrections to the λ parameters, mentioned earlier, are also included in the selection systematic uncertainty. Taking the upper-limit values of the variations to be conservative, this led to additional uncertainties of 4% for R and 8% for λ . As seen in Table 3, the fit systematic uncertainty tends to be comparable to or larger than the selection systematic uncertainty, reflecting the scale of uncertainties in determining the non-femtoscopic baseline in pp collisions. The “total quadratic uncertainty” is the square-root of the quadratic sum of the “statistical uncertainty” column and the “total systematic uncertainty” column.

4.4 Momentum resolution

Finite track momentum resolution can smear the relative momentum correlation functions used in this analysis. This effect was taken into account using PYTHIA8+GEANT MC simulations. Two PYTHIA8 correlation functions are built using the generator-level momentum (k_{ideal}^*) and the measured detector-level momentum (k_{meas}^*). Because PYTHIA8 does not incorporate final-state interactions, weights are calculated using a 9th-order polynomial fit in k^* to an experimental correlation function and used when filling the same-event distributions. These weights are calculated using k_{ideal}^* . Then, the ratio of the “ideal” correlation function to the “measured” one for each k^* bin is multiplied by the data correlation functions before the fit procedure. It is found that, due to the large k^* bin size of 20 MeV/ c which is used in the analysis of pp collisions, the correction has a small effect on the lowest k^* bin with the largest statistical error bars, and a negligible effect on the remaining bins. Thus, the momentum resolution correction was found to have a $< 2\%$ effect on the extracted fit parameters.

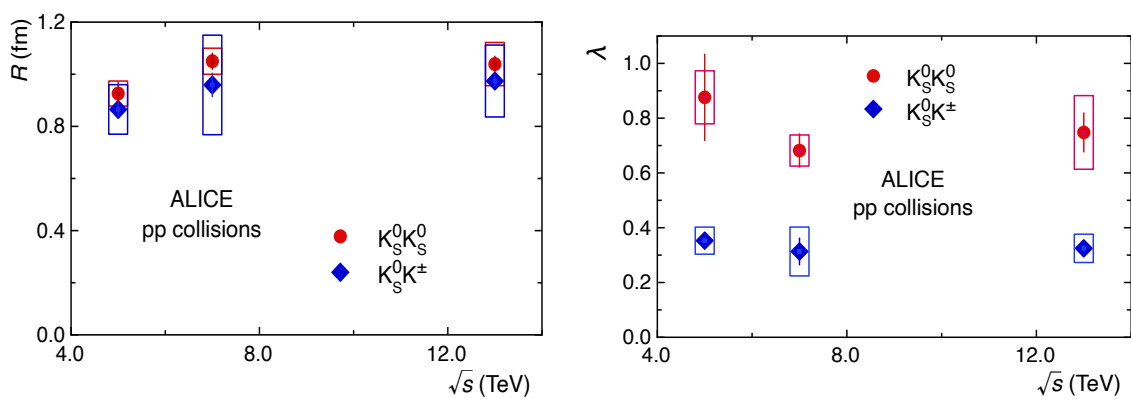
5 Results and discussion

The extracted source parameters for $K_S^0 K_S^0$ and $K_S^0 K^\pm$, where $K_S^0 K^+$ and $K_S^0 K^-$ have been summed over, are shown in Table 3 and in Figure 6. The λ parameters are corrected for particle-pair purity. Figure 6 shows comparisons of the present results for R and λ in pp collisions at $\sqrt{s} = 5.02$ and 13 TeV with published two-kaon femtoscopic results measured in pp collisions at $\sqrt{s} = 7$ TeV [6].

For the R parameters, two observations can clearly be made: 1) there is no significant dependence on \sqrt{s} , i.e. all extracted values are ~ 1 fm, and 2) the values extracted from $K_S^0 K_S^0$ and $K_S^0 K^\pm$ for a given \sqrt{s} agree within uncertainties, as would be expected. It is expected that R from $K_S^0 K_S^0$ and $K_S^0 K^\pm$ would agree with each other if a) the K_S^0 and K^\pm are produced in the same source geometry, and b) Eqs. 6 and 7 properly describe the pair interactions. Point a) is expected to be true due to isospin invariance of the strong interaction that produces the kaons in the pp collision, and point b) is supported by the overall good fits that Eqs. 6 and 7 are seen to give to the experimental correlation functions. The R

Table 3: Fit results for average R and λ along with statistical and systematic uncertainties. The λ parameters are corrected for particle-pair purity.

R or λ kaon pair	pp energy (TeV)	fit value	statistical uncert. (\pm)	fit systematic uncert. (\pm)	selection systematic uncert. (\pm)	total systematic uncert. (\pm)	total quadratic uncert. (\pm)
R (fm) $K_S^0 K_S^0$	5.02	0.926	0.045	0.031	0.037	0.048	0.066
λ $K_S^0 K_S^0$	5.02	0.876	0.159	0.067	0.070	0.097	0.186
R (fm) $K_S^0 K^\pm$	5.02	0.865	0.025	0.088	0.037	0.095	0.098
λ $K_S^0 K^\pm$	5.02	0.353	0.031	0.039	0.029	0.049	0.058
R (fm) $K_S^0 K_S^0$	13	1.039	0.032	0.072	0.042	0.083	0.089
λ $K_S^0 K_S^0$	13	0.748	0.073	0.121	0.059	0.134	0.153
R (fm) $K_S^0 K^\pm$	13	0.974	0.020	0.131	0.042	0.138	0.139
λ $K_S^0 K^\pm$	13	0.325	0.020	0.044	0.028	0.052	0.055


Figure 6: R (left) and λ (right) parameters extracted in the present analysis from Table 3 compared with published $K_S^0 K_S^0$ and $K_S^0 K^\pm$ results from ALICE 7 TeV pp collisions [6] averaged over event multiplicity and evaluated at $\langle k_T \rangle = 0.6$ GeV/ c . Statistical uncertainties are shown as error bars and the systematic uncertainties are shown as boxes.

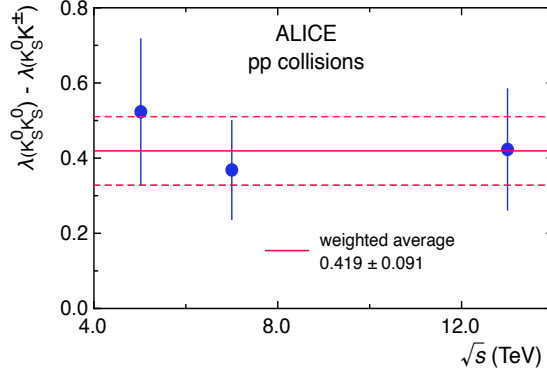


Figure 7: Differences in λ parameters extracted in the present analysis from Table 3 compared with published identical and non-identical kaon results from ALICE 7 TeV pp collisions averaged over event multiplicity and evaluated at $\langle k_T \rangle = 0.6$ GeV/ c . Total uncertainties are shown. The weighted average of the differences is shown as a solid red line and the weighted uncertainty, $\pm\sigma$, shown as red dashed lines.

parameter is essentially independent of \sqrt{s} . While R in general depends on pseudorapidity density also in pp collisions [28–30], the increase expected from the slow logarithmic rise of pseudorapidity density with \sqrt{s} is well within our experimental uncertainties.

The extracted λ parameters in Fig. 6 suggest that: 1) the values do not depend significantly on \sqrt{s} , 2) the values for $K_S^0 K_S^0$ are in the usual range seen in femtoscopy experiments of $\lambda \sim 0.7$ – 0.8 , whereas 3) the values for $K_S^0 K^\pm$ are significantly smaller being $\lambda \sim 0.3$ – 0.4 , consistent with the 7 TeV results. Figure 7 shows the difference between purity-corrected λ parameters extracted with $K_S^0 K_S^0$ and $K_S^0 K^\pm$ versus \sqrt{s} . The propagated total uncertainty is indicated on these points. Also shown is the weighted average of these points, weighted by their total uncertainties. It is assumed that the total uncertainties of the $K_S^0 K_S^0$ and $K_S^0 K^\pm$ measurements are uncorrelated. This is considered a reasonable assumption given the differences in the kaon pairs and the equations used to extract the source parameters. The weighted average of the differences is calculated to be 0.419 ± 0.091 , which is 4.6σ from zero.

There are three main technical factors that, while having a small effect on the R parameter, can significantly affect the value of the λ parameter: 1) the experimental kaon reconstruction purity, 2) the degree to which a Gaussian distribution describes the kaon source, and 3) the presence of kaons originating from the decay of long-lived resonances diluting the direct-kaon sample [6]. The effect of factor 1) is already corrected for by having divided the extracted λ values by the products of the single-kaon purities given in Section 2.1. As seen in Figs. 4 and 5, the Lednický equation, which uses a Gaussian source, fits the experimental correlation functions well, an observation that is supported by the good χ^2/ndf values given above, minimizing the effect of 2). The effects from factor 3) are discussed in the following section.

5.1 Effect of presence of long-lived resonances

Table 4 gives a list of mesons from the Review of Particle Physics [34] with masses < 1500 MeV/ c^2 that have decay channels into kaons with significant branching ratios. The two lowest-lying mesons, the $K^*(892)$ and the $\phi(1020)$, are the most abundantly produced and have the narrowest widths, and so are expected to have the greatest effect on the values of the extracted kaon source parameters, which reflect both the kaons produced from the decays of resonances as well as the kaons produced directly from the pp collision. Since the mean decay lengths of the K^* and ϕ are about 4 fm and 50 fm, respectively (see Table 4), these decays result in effective sources of kaons which are much larger than the expected size of the direct kaon source in pp collisions of about 1 fm. Thus, the effect of these should be mostly to reduce the extracted λ parameter. This is due to the correlation function for the smaller-sized direct source being wider in k^* and so dominating the extracted R [35]. Thus, the kaons from these resonances only make an overall suppression of the correlation function.

Table 4: List of mesons from the Review of Particle Physics [34] with masses $< 1500 \text{ MeV}/c^2$ that have decay channels into kaons with significant branching ratios.

Name	mass (MeV/c^2)	Γ (MeV/c^2)	kaon decays	$\hbar c/\Gamma$ (fm)
$K^*(892)$	891.67	51.4	$K\pi$ (100%)	3.839
$\phi(1020)$	1019.46	4.249	$K^+ K^-$ (49.2%), $K_L^0 K_S^0$ (34%)	46.4
$K_1(1270)$	1253	~ 100	$K\rho$ (42%)	1.973
$K_0^*(1430)$	1425	270	$K\pi$ ($\sim 100\%$)	0.731
$K_2^*(1430)$	1427.3	100	$K\pi$ (50%), KX (12%)	1.973

Table 5: ALICE measurements of $K^*(892)/K$ and $\phi(1020)/K$ ratios. The uncertainties given are the statistical and systematic uncertainties combined in quadrature.

Ref.	collision	$K^*(892)/K$	$\phi(1020)/K$	average p_T (GeV/c)	trigger
[36]	2.76 TeV pp	$K^{*0}/K^- 0.31 \pm 0.04$	$\phi/K^- 0.11 \pm 0.01$	~ 1	inelastic
[37]	7 TeV pp	$K^{*0}/K^- 0.35 \pm 0.04$	$\phi/K^- 0.11 \pm 0.02$	~ 1	inelastic
[38]	13 TeV pp	$K^{*0}/K_S^0 0.34 \pm 0.01$	$\phi/K_S^0 0.11 \pm 0.01$	0.6	low multiplicity
[39]	5.02 TeV pp	$K^{*0}/K^\pm 0.29 \pm 0.02$	$\phi/K^\pm 0.08 \pm 0.02$	~ 0.6	inelastic

Table 6: Decay modes of the charge states of the $K^*(892)$. Note that the K^0 is made up of 50% K_S^0 and 50% K_L^0 .

$K^*(892)$ charge state	decay channels	comment
K^{*+}	$K^+ \pi^0, K^0 \pi^+$	each channel 50%
K^{*-}	$K^- \pi^0, K^0 \pi^-$	each channel 50%
K^{*0}, \bar{K}^{*0}	$K^+ \pi^-, K^- \pi^+, K^0 \pi^0$	each channel 33.3%

The dilution effect on the λ parameter due to the $K^*(892)$ and $\phi(1020)$ decays can be estimated from K^{*0}/K and ϕ/K ratio measurements from ALICE [36–39]. Table 5 shows the measurements of these quantities relevant to the present estimate. As shown in the table, the measured ratios for both K^{*0}/K and ϕ/K are independent of the collision energy and independent of the decay-kaon charge state within the measurement uncertainties. For the present calculation, the ratios from Refs. [38, 39] are used since they are taken with an average p_T close to the average k_T of 0.6 GeV/c used in this analysis. Whereas the ϕ only has one charge state for each of its decay channels, as seen in Table 4, and is its own anti-particle, the K^* has four charge states, and three unique sets of decay charge-state channels, as shown in Table 6, which is taken into account in the present calculation. Using the numbers in Tables 4, 5, and 6, the direct-kaon purity for K^+ , K^- and K_S^0 , defined as $P(K^+)$, $P(K^-)$ and $P(K_S^0)$, respectively, where $P(K^+) = P(K^-) \equiv P(K^\pm)$, are calculated to be $P(K^\pm) = 0.726$, and $P(K_S^0) = 0.757$.

In the calculations, it has been assumed that the ratios $K^{*0}/K^\pm = K^{*\pm}/K^\pm$ and $K^{*0}/K_S^0 = K^{*\pm}/K_S^0$. The ‘‘diluted’’ λ parameters can then be estimated for $K_S^0 K_S^0$ as $P(K_S^0)P(K_S^0) = 0.57 \pm 0.02$ and for $K_S^0 K^\pm$ as $P(K_S^0)P(K^\pm) = 0.55 \pm 0.02$. The effect of these long-lived resonances is seen to be of the same magnitude, within the uncertainties, for $K_S^0 K_S^0$ and $K_S^0 K^\pm$. The estimate is ~ 1 – 2σ lower than the purity-corrected λ values measured with $K_S^0 K_S^0$, however it is ~ 3 – 4σ larger than the values measured in $K_S^0 K^\pm$. Thus, the dilution effects on λ by the $K^*(892)$ and $\phi(1020)$ cannot explain the small values for λ measured in pp collisions in $K_S^0 K^\pm$ femtoscopy.

5.2 Physics explanations for differences of λ parameters

Since the technical factors discussed above affecting the extracted λ values should affect the values from $K_S^0 K_S^0$ and $K_S^0 K^\pm$ in the same way, their difference can be ascribed to a physics effect. It is important to first compare the λ parameters extracted in the present work to those measured in other published KK femtoscopic studies. In Pb–Pb collisions, λ is measured to be ~ 0.7 for $K_S^0 K_S^0$, $K^\pm K^\pm$ and $K_S^0 K^\pm$ [7], similar to what is measured for $K_S^0 K_S^0$ presented here, and close to the estimate made for the resonance

dilution effect. For $K^\pm K^\pm$ femtoscopy in pp and pPb collisions, λ is measured to be in the range 0.4–0.5, which is smaller than for $K_S^0 K_S^0$ presented here [40]. Note that one expects $K^\pm K^\pm$ to be somewhat smaller than $K_S^0 K_S^0$ on the basis of the resonance dilution effect, since for $K^\pm K^\pm$ the λ is estimated to be $P(K^\pm)P(K^\pm) = 0.53$ as compared with $P(K_S^0)P(K_S^0) = 0.57$ estimated for $K_S^0 K_S^0$. As to why the λ parameters in $K^\pm K^\pm$ in pp and p–Pb collisions are smaller than in Pb–Pb collisions, Ref. [40] suggests that this could be due to the kaon source being more Gaussian in Pb–Pb collisions.

As discussed in Ref. [6], a physics effect that could cause the difference in λ values is related to the possibility that the a_0 resonance, that is solely responsible for the FSI in the $K_S^0 K^\pm$ pair, is a tetraquark state of the form $(q_1, \bar{q}_2, s, \bar{s})$ instead of a diquark state of the form (q_1, \bar{q}_2) , where q_1 and q_2 are u or d quarks. The strength of the FSI through a tetraquark a_0 could be decreased by the small source size of the kaon source, i.e. $R \sim 1$ fm as measured in this analysis, since $s - \bar{s}$ annihilation would be enhanced due to the close creation proximity. For a FSI through a diquark a_0 , with the form (q_1, \bar{q}_2) , the small source geometry should not reduce its strength. For the $K_S^0 K_S^0$ case, λ would not be affected much by a tetraquark a_0 since the enhancement in the correlation function near $k^* \sim 0$ is dominated by the effect of quantum statistics. Note that for the large kaon source measured in Pb–Pb collisions to have $R \sim 6$ fm, the situation would be reversed. The large average separation between the kaons would favor the formation of a tetraquark a_0 and suppress the formation of a diquark a_0 , and a larger $\lambda \sim 0.6$ is indeed measured in that case, as already mentioned above. Thus, we can conclude that, as was the case with the published $\sqrt{s} = 7$ TeV result, the present results in pp collisions at $\sqrt{s} = 5.02$ and 13 TeV are compatible with the a_0 being a tetraquark state.

6 Summary

In summary, femtosopic correlations with the particle pair combinations $K_S^0 K_S^0$ and $K_S^0 K^\pm$ are studied in pp collisions at $\sqrt{s} = 5.02$ and 13 TeV for the first time by the ALICE experiment at the LHC. By fitting models that assume a Gaussian size distribution of the kaon source to the experimental two-particle correlation functions, kaon source parameters are extracted. The model used for the $K_S^0 K_S^0$ case includes quantum statistics and strong final-state interactions through the f_0 and a_0 resonances. The model used for the $K_S^0 K^\pm$ case involves only the final-state interaction through the a_0 resonance. In both cases, the models gave a good fit to the experimental correlation functions. Source parameters extracted in the present work are compared with published values from ALICE measured in pp collisions at $\sqrt{s} = 7$ TeV and found to be consistent, i.e. there is no significant dependence of either R or λ on the collision energy. The new results are compatible with the a_0 resonance being a tetraquark state due to the λ parameter for $K_S^0 K^\pm$ being significantly smaller than for $K_S^0 K_S^0$.

Acknowledgements

The ALICE Collaboration would like to thank all its engineers and technicians for their invaluable contributions to the construction of the experiment and the CERN accelerator teams for the outstanding performance of the LHC complex. The ALICE Collaboration gratefully acknowledges the resources and support provided by all Grid centres and the Worldwide LHC Computing Grid (WLCG) collaboration. The ALICE Collaboration acknowledges the following funding agencies for their support in building and running the ALICE detector: A. I. Alikhanyan National Science Laboratory (Yerevan Physics Institute) Foundation (ANSL), State Committee of Science and World Federation of Scientists (WFS), Armenia; Austrian Academy of Sciences, Austrian Science Fund (FWF): [M 2467-N36] and Nationalstiftung für Forschung, Technologie und Entwicklung, Austria; Ministry of Communications and High Technologies, National Nuclear Research Center, Azerbaijan; Conselho Nacional de Desenvolvimento Científico e Tecnológico (CNPq), Financiadora de Estudos e Projetos (Finep), Fundação de Amparo à Pesquisa do Estado de São Paulo (FAPESP) and Universidade Federal do Rio Grande do Sul (UFRGS),

Brazil; Ministry of Education of China (MOEC), Ministry of Science & Technology of China (MSTC) and National Natural Science Foundation of China (NSFC), China; Ministry of Science and Education and Croatian Science Foundation, Croatia; Centro de Aplicaciones Tecnológicas y Desarrollo Nuclear (CEADEN), Cubaenergía, Cuba; Ministry of Education, Youth and Sports of the Czech Republic, Czech Republic; The Danish Council for Independent Research | Natural Sciences, the VILLUM FONDEN and Danish National Research Foundation (DNRF), Denmark; Helsinki Institute of Physics (HIP), Finland; Commissariat à l’Energie Atomique (CEA) and Institut National de Physique Nucléaire et de Physique des Particules (IN2P3) and Centre National de la Recherche Scientifique (CNRS), France; Bundesministerium für Bildung und Forschung (BMBF) and GSI Helmholtzzentrum für Schwerionenforschung GmbH, Germany; General Secretariat for Research and Technology, Ministry of Education, Research and Religions, Greece; National Research, Development and Innovation Office, Hungary; Department of Atomic Energy Government of India (DAE), Department of Science and Technology, Government of India (DST), University Grants Commission, Government of India (UGC) and Council of Scientific and Industrial Research (CSIR), India; Indonesian Institute of Science, Indonesia; Istituto Nazionale di Fisica Nucleare (INFN), Italy; Japanese Ministry of Education, Culture, Sports, Science and Technology (MEXT), Japan Society for the Promotion of Science (JSPS) KAKENHI and Japanese Ministry of Education, Culture, Sports, Science and Technology (MEXT) of Applied Science (IIST), Japan; Consejo Nacional de Ciencia (CONACYT) y Tecnología, through Fondo de Cooperación Internacional en Ciencia y Tecnología (FONCICYT) and Dirección General de Asuntos del Personal Académico (DGAPA), Mexico; Nederlandse Organisatie voor Wetenschappelijk Onderzoek (NWO), Netherlands; The Research Council of Norway, Norway; Commission on Science and Technology for Sustainable Development in the South (COMSATS), Pakistan; Pontificia Universidad Católica del Perú, Peru; Ministry of Education and Science, National Science Centre and WUT ID-UB, Poland; Korea Institute of Science and Technology Information and National Research Foundation of Korea (NRF), Republic of Korea; Ministry of Education and Scientific Research, Institute of Atomic Physics, Ministry of Research and Innovation and Institute of Atomic Physics and University Politehnica of Bucharest, Romania; Joint Institute for Nuclear Research (JINR), Ministry of Education and Science of the Russian Federation, National Research Centre Kurchatov Institute, Russian Science Foundation and Russian Foundation for Basic Research, Russia; Ministry of Education, Science, Research and Sport of the Slovak Republic, Slovakia; National Research Foundation of South Africa, South Africa; Swedish Research Council (VR) and Knut & Alice Wallenberg Foundation (KAW), Sweden; European Organization for Nuclear Research, Switzerland; Suranaree University of Technology (SUT), National Science and Technology Development Agency (NSDTA) and Office of the Higher Education Commission under NRU project of Thailand, Thailand; Turkish Energy, Nuclear and Mineral Research Agency (TENMAK), Turkey; National Academy of Sciences of Ukraine, Ukraine; Science and Technology Facilities Council (STFC), United Kingdom; National Science Foundation of the United States of America (NSF) and United States Department of Energy, Office of Nuclear Physics (DOE NP), United States of America.

References

- [1] M. A. Lisa, S. Pratt, R. Soltz, and U. Wiedemann, “Femtoscopy in relativistic heavy ion collisions”, *Ann. Rev. Nucl. Part. Sci.* **55** (2005) 357–402, arXiv:nucl-ex/0505014 [nucl-ex].
- [2] **STAR** Collaboration, B. I. Abelev *et al.*, “Neutral kaon interferometry in Au+Au collisions at $\sqrt{s_{NN}} = 200$ GeV”, *Phys. Rev.* **C74** (2006) 054902, arXiv:nucl-ex/0608012 [nucl-ex].
- [3] **ALICE** Collaboration, B. Abelev *et al.*, “K_s⁰ – K_s⁰ correlations in pp collisions at $\sqrt{s} = 7$ TeV from the LHC ALICE experiment”, *Phys. Lett.* **B717** (2012) 151–161, arXiv:1206.2056 [hep-ex].
- [4] **ALICE** Collaboration, B. Abelev *et al.*, “Charged kaon femtoscopic correlations in pp collisions at $\sqrt{s} = 7$ TeV”, *Phys. Rev.* **D87** (2013) 052016, arXiv:1212.5958 [hep-ex].

- [5] **ALICE** Collaboration, J. Adam *et al.*, “One-dimensional pion, kaon, and proton femtoscopy in Pb-Pb collisions at $\sqrt{s_{NN}}=2.76$ TeV”, *Phys. Rev.* **C92** (2015) 054908, arXiv:1506.07884 [nucl-ex].
- [6] **ALICE** Collaboration, S. Acharya *et al.*, “Measuring $K_S^0 K^\pm$ interactions using pp collisions at $\sqrt{s} = 7$ TeV”, *Phys. Lett.* **B790** (2019) 22–34, arXiv:1809.07899 [nucl-ex].
- [7] **ALICE** Collaboration, S. Acharya *et al.*, “Measuring $K_S^0 K^\pm$ interactions using Pb-Pb collisions at $\sqrt{s_{NN}} = 2.76$ TeV”, *Phys. Lett. B* **774** (2017) 64–77, arXiv:1705.04929 [nucl-ex].
- [8] **NPLQCD** Collaboration, S. R. Beane *et al.*, “The $K^+ K^+$ scattering length from lattice QCD”, *Phys. Rev.* **D77** (2008) 094507, arXiv:0709.1169 [hep-lat].
- [9] R. L. Jaffe, “Multi-Quark Hadrons. 1. The Phenomenology of $qq\bar{q}\bar{q}$ Mesons”, *Phys. Rev.* **D15** (1977) 267.
- [10] M. G. Alford and R. L. Jaffe, “Insight into the scalar mesons from a lattice calculation”, *Nucl. Phys.* **B578** (2000) 367–382, arXiv:hep-lat/0001023 [hep-lat].
- [11] E. Santopinto and G. Galata, “Spectroscopy of tetraquark states”, *Phys. Rev.* **C75** (2007) 045206, arXiv:hep-ph/0605333 [hep-ph].
- [12] S. Narison, “Light scalar mesons in QCD”, *Nucl. Phys. B Proc. Suppl.* **186** (2009) 306–311, arXiv:0811.0563 [hep-ph].
- [13] N. Achasov and A. Kiselev, “Light scalar mesons and two-kaon correlation functions”, *Phys. Rev. D* **97** (2018) 036015, arXiv:1711.08777 [hep-ph].
- [14] K. Azizi, B. Barsbay, and H. Sundu, “Light scalar $K_0^*(700)$ meson in vacuum and a hot medium”, *Phys. Rev. D* **100** (2019) 094041, arXiv:1909.00716 [hep-ph].
- [15] **Hadron Spectrum** Collaboration, J. J. Dudek, R. G. Edwards, and D. J. Wilson, “An a_0 resonance in strongly coupled $\pi\eta$, $K\bar{K}$ scattering from lattice QCD”, *Phys. Rev. D* **93** (2016) 094506, arXiv:1602.05122 [hep-ph].
- [16] R. A. Briceno, J. J. Dudek, R. G. Edwards, and D. J. Wilson, “Isoscalar $\pi\pi$ scattering and the σ meson resonance from QCD”, *Phys. Rev. Lett.* **118** (2017) 022002, arXiv:1607.05900 [hep-ph].
- [17] F.-K. Guo, L. Liu, U.-G. Meissner, and P. Wang, “Tetraquarks, hadronic molecules, meson-meson scattering and disconnected contributions in lattice QCD”, *Phys. Rev. D* **88** (2013) 074506, arXiv:1308.2545 [hep-lat].
- [18] **ALICE** Collaboration, K. Aamodt *et al.*, “The ALICE experiment at the CERN LHC”, *JINST* **3** (2008) S08002.
- [19] T. Sjostrand, S. Mrenna, and P. Skands, “PYTHIA 6.4 Physics and Manual”, *JHEP* **05** (2006) 026, arXiv:hep-ph/0603175.
- [20] P. Skands, S. Carrazza, and J. Rojo, “Tuning PYTHIA 8.1: the Monash 2013 Tune”, *Eur. Phys. J. C* **74** (2014) 3024, arXiv:1404.5630 [hep-ph].
- [21] R. Brun, F. Bruyant, F. Carminati, S. Giani, M. Maire, A. McPherson, G. Patrick, and L. Urban, “GEANT Detector Description and Simulation Tool”, *CERN Document Server* (10, 1994).
- [22] **ALICE** Collaboration, B. Abelev *et al.*, “Centrality dependence of π , K, p production in Pb-Pb collisions at $\sqrt{s_{NN}} = 2.76$ TeV”, *Phys. Rev.* **C88** (2013) 044910, arXiv:1303.0737 [hep-ex].

- [23] ALICE Collaboration, B. Abelev *et al.*, “Centrality determination of Pb-Pb collisions at $\sqrt{s_{NN}}=2.76$ TeV with ALICE”, *Phys. Rev.* **C88** (2013) 044909, arXiv:1301.4361 [nucl-ex].
- [24] J. Alme *et al.*, “The ALICE TPC, a large 3-dimensional tracking device with fast readout for ultra-high multiplicity events”, *Nucl. Instrum. Meth.* **A622** (2010) 316–367, arXiv:1001.1950 [physics.ins-det].
- [25] ALICE Collaboration, B. Alessandro *et al.*, “ALICE: Physics performance report, volume II”, *J. Phys.* **G32** (2006) 1295–2040.
- [26] ALICE Collaboration, B. B. Abelev *et al.*, “Performance of the ALICE Experiment at the CERN LHC”, *Int. J. Mod. Phys.* **A29** (2014) 1430044, arXiv:1402.4476 [nucl-ex].
- [27] A. Akindinov *et al.*, “Performance of the ALICE Time-Of-Flight detector at the LHC”, *Eur. Phys. J. Plus* **128** (2013) 44.
- [28] ALICE Collaboration, S. Acharya *et al.*, “Event-shape and multiplicity dependence of freeze-out radii in pp collisions at $\sqrt{s} = 7$ TeV”, *JHEP* **09** (2019) 108, arXiv:1901.05518 [nucl-ex].
- [29] ALICE Collaboration, S. Acharya *et al.*, “Charged-particle production as a function of multiplicity and transverse sphericity in pp collisions at $\sqrt{s} = 5.02$ and 13 TeV”, *Eur. Phys. J. C* **79** (2019) 857, arXiv:1905.07208 [nucl-ex].
- [30] ALICE Collaboration, K. Aamodt *et al.*, “Charged-particle multiplicity measurement in proton-proton collisions at $\sqrt{s} = 7$ TeV with ALICE at LHC”, *Eur. Phys. J. C* **68** (2010) 345–354, arXiv:1004.3514 [hep-ex].
- [31] R. Lednický and V. Lyuboshits, “Final State Interaction Effect on Pairing Correlations Between Particles with Small Relative Momenta”, *Sov. J. Nucl. Phys.* **35** (1982) 770.
- [32] R. Lednický, “Correlation femtoscopy”, *Nucl. Phys.* **A774** (2006) 189–198, arXiv:nucl-th/0510020 [nucl-th].
- [33] N. N. Achasov and A. V. Kiselev, “The New analysis of the KLOE data on the $\phi \rightarrow \eta \pi^0$ gamma decay”, *Phys. Rev.* **D68** (2003) 014006, arXiv:hep-ph/0212153 [hep-ph].
- [34] Particle Data Group Collaboration, P. A. Zyla *et al.*, “Review of Particle Physics”, *PTEP* **2020** (2020) 083C01.
- [35] T. J. Humanic, “Hanbury-brown-twiss interferometry with identical bosons in relativistic heavy ion collisions: Comparisons with hadronic scattering models”, *Int. J. Mod. Phys.* **E15** (2006) 197–236, nucl-th/0510049.
- [36] ALICE Collaboration, J. Adam *et al.*, “K*(892)⁰ and $\phi(1020)$ meson production at high transverse momentum in pp and Pb-Pb collisions at $\sqrt{s_{NN}} = 2.76$ TeV”, *Phys. Rev. C* **95** (2017) 064606, arXiv:1702.00555 [nucl-ex].
- [37] ALICE Collaboration, B. Abelev *et al.*, “Production of K*(892)⁰ and $\phi(1020)$ in pp collisions at $\sqrt{s} = 7$ TeV”, *Eur. Phys. J.* **C72** (2012) 2183, arXiv:1208.5717 [hep-ex].
- [38] ALICE Collaboration, S. Acharya *et al.*, “Multiplicity dependence of K*(892)⁰ and $\phi(1020)$ production in pp collisions at $\sqrt{s} = 13$ TeV”, *Phys. Lett. B* **807** (2020) 135501, arXiv:1910.14397 [nucl-ex].
- [39] ALICE Collaboration, S. Acharya *et al.*, “Evidence of rescattering effect in Pb-Pb collisions at the LHC through production of K*(892)⁰ and $\phi(1020)$ mesons”, *Phys. Lett. B* **802** (2020) 135225, arXiv:1910.14419 [nucl-ex].

- [40] **ALICE** Collaboration, S. Acharya *et al.*, “One-dimensional charged kaon femtoscopy in p-Pb collisions at $\sqrt{s_{NN}} = 5.02$ TeV”, *Phys. Rev. C* **100** (2019) 024002, arXiv:1903.12310 [nucl-ex].

A The ALICE Collaboration

S. Acharya¹⁴³, D. Adamová⁹⁷, A. Adler⁷⁵, J. Adolfsson⁸², G. Aglieri Rinella³⁴, M. Agnello³⁰, N. Agrawal⁵⁴, Z. Ahammed¹⁴³, S. Ahmad¹⁶, S.U. Ahn⁷⁷, I. Ahuja³⁸, Z. Akbar⁵¹, A. Akindinov⁹⁴, M. Al-Turany¹⁰⁹, S.N. Alam¹⁶, D. Aleksandrov⁹⁰, B. Alessandro⁶⁰, H.M. Alfanda⁷, R. Alfaro Molina⁷², B. Ali¹⁶, Y. Ali¹⁴, A. Alici²⁵, N. Alizadehvandchali¹²⁶, A. Alkin³⁴, J. Alme²¹, G. Alocco⁵⁵, T. Alt⁶⁹, I. Altsybeev¹¹⁴, M.N. Anaam⁷, C. Andrei⁴⁸, D. Andreou⁹², A. Andronic¹⁴⁶, M. Angeletti³⁴, V. Angelov¹⁰⁶, F. Antinori⁵⁷, P. Antonioli⁵⁴, C. Anuj¹⁶, N. Apadula⁸¹, L. Aphecetche¹¹⁶, H. Appelshäuser⁶⁹, S. Arcelli²⁵, R. Arnaldi⁶⁰, I.C. Arsene²⁰, M. Arslandok¹⁴⁸, A. Augustinus³⁴, R. Averbeck¹⁰⁹, S. Aziz⁷⁹, M.D. Azmi¹⁶, A. Badalà⁵⁶, Y.W. Baek⁴¹, X. Bai^{130,109}, R. Bailhache⁶⁹, Y. Bailung⁵⁰, R. Bala¹⁰³, A. Balbino³⁰, A. Baldisseri¹⁴⁰, B. Balis², D. Banerjee⁴, Z. Banoo¹⁰³, R. Barbera²⁶, L. Barioglio¹⁰⁷, M. Barlou⁸⁶, G.G. Barnaföldi¹⁴⁷, L.S. Barnby⁹⁶, V. Barret¹³⁷, C. Bartels¹²⁹, K. Barth³⁴, E. Bartsch⁶⁹, F. Baruffaldi²⁷, N. Bastid¹³⁷, S. Basu⁸², G. Batigne¹¹⁶, B. Batyunya⁷⁶, D. Bauri⁴⁹, J.L. Bazo Alba¹¹³, I.G. Bearden⁹¹, C. Beattie¹⁴⁸, P. Becht¹⁰⁹, I. Belikov¹³⁹, A.D.C. Bell Hechavarria¹⁴⁶, F. Bellini²⁵, R. Bellwied¹²⁶, S. Belokurova¹¹⁴, V. Belyaev⁹⁵, G. Bencedi^{147,70}, S. Beole²⁴, A. Bercuci⁴⁸, Y. Berdnikov¹⁰⁰, A. Berdnikova¹⁰⁶, L. Bergmann¹⁰⁶, M.G. Besoiu⁶⁸, L. Betev³⁴, P.P. Bhaduri¹⁴³, A. Bhasin¹⁰³, I.R. Bhat¹⁰³, M.A. Bhat⁴, B. Bhattacharjee⁴², P. Bhattacharya²², L. Bianchi²⁴, N. Bianchi⁵², J. Bielčik³⁷, J. Bielčiková⁹⁷, J. Biernat¹¹⁹, A. Bilandzic¹⁰⁷, G. Biro¹⁴⁷, S. Biswas⁴, J.T. Blair¹²⁰, D. Blau^{90,83}, M.B. Blidar¹⁰⁹, C. Blume⁶⁹, G. Boca^{28,58}, F. Bock⁹⁸, A. Bogdanov⁹⁵, S. Boi²², J. Bok⁶², L. Boldizsár¹⁴⁷, A. Bolozdynya⁹⁵, M. Bombara³⁸, P.M. Bond³⁴, G. Bonomi^{142,58}, H. Borel¹⁴⁰, A. Borissov⁸³, H. Bossi¹⁴⁸, E. Botta²⁴, L. Bratrud⁶⁹, P. Braun-Munzinger¹⁰⁹, M. Bregant¹²², M. Broz³⁷, G.E. Bruno^{108,33}, M.D. Buckland^{23,129}, D. Budnikov¹¹⁰, H. Buesching⁶⁹, S. Bufalino³⁰, O. Bugnon¹¹⁶, P. Buhler¹¹⁵, Z. Buthelezi^{73,133}, J.B. Butt¹⁴, A. Bylinkin¹²⁸, S.A. Bysiak¹¹⁹, M. Cai^{27,7}, H. Caines¹⁴⁸, A. Caliva¹⁰⁹, E. Calvo Villar¹¹³, J.M.M. Camacho¹²¹, R.S. Camacho⁴⁵, P. Camerini²³, F.D.M. Canedo¹²², F. Carnesecchi^{34,25}, R. Caron¹⁴⁰, J. Castillo Castellanos¹⁴⁰, E.A.R. Casula²², F. Catalano³⁰, C. Ceballos Sanchez⁷⁶, P. Chakraborty⁴⁹, S. Chandra¹⁴³, S. Chapeland³⁴, M. Chartier¹²⁹, S. Chattopadhyay¹⁴³, S. Chattopadhyay¹¹¹, T.G. Chavez⁴⁵, T. Cheng⁷, C. Cheshkov¹³⁸, B. Cheynis¹³⁸, V. Chibante Barroso³⁴, D.D. Chinellato¹²³, S. Cho⁶², P. Chochula³⁴, P. Christakoglou⁹², C.H. Christensen⁹¹, P. Christiansen⁸², T. Chujo¹³⁵, C. Cicalo⁵⁵, L. Cifarelli²⁵, F. Cindolo⁵⁴, M.R. Ciupek¹⁰⁹, G. Clai^{II,54}, J. Cleymans^{I,125}, F. Colamaria⁵³, J.S. Colburn¹¹², D. Colella^{53,108,33}, A. Collu⁸¹, M. Colocci³⁴, M. Concas^{III,60}, G. Conesa Balbastre⁸⁰, Z. Conesa del Valle⁷⁹, G. Contin²³, J.G. Contreras³⁷, M.L. Coquet¹⁴⁰, T.M. Cormier⁹⁸, P. Cortese³¹, M.R. Cosentino¹²⁴, F. Costa³⁴, S. Costanza^{28,58}, P. Crochet¹³⁷, R. Cruz-Torres⁸¹, E. Cuautle⁷⁰, P. Cui⁷, L. Cunqueiro⁹⁸, A. Dainese⁵⁷, M.C. Danisch¹⁰⁶, A. Danu⁶⁸, P. Das⁸⁸, P. Das⁴, S. Das⁴, S. Dash⁴⁹, A. De Caro²⁹, G. de Cataldo⁵³, L. De Cilladi²⁴, J. de Cuveland³⁹, A. De Falco²², D. De Gruttola²⁹, N. De Marco⁶⁰, C. De Martin²³, S. De Pasquale²⁹, S. Deb⁵⁰, H.F. Degenhardt¹²², K.R. Deja¹⁴⁴, R. Del Grande¹⁰⁷, L. Dello Stritto²⁹, W. Deng⁷, P. Dhankher¹⁹, D. Di Bari³³, A. Di Mauro³⁴, R.A. Diaz⁸, T. Dietel¹²⁵, Y. Ding^{138,7}, R. Divià³⁴, D.U. Dixit¹⁹, Ø. Djuvsland²¹, U. Dmitrieva⁶⁴, J. Do⁶², A. Dobrin⁶⁸, B. Dönigus⁶⁹, A.K. Dubey¹⁴³, A. Dubla^{109,92}, S. Dudi¹⁰², P. Dupieux¹³⁷, N. Dzalaiova¹³, T.M. Eder¹⁴⁶, R.J. Ehlers⁹⁸, V.N. Eikeland²¹, F. Eisenhut⁶⁹, D. Elia⁵³, B. Erasmus¹¹⁶, F. Ercolessi²⁵, F. Erhardt¹⁰¹, A. Erokhin¹¹⁴, M.R. Ersdal²¹, B. Espagnon⁷⁹, G. Eulisse³⁴, D. Evans¹¹², S. Evdokimov⁹³, L. Fabbietti¹⁰⁷, M. Faggin²⁷, J. Faivre⁸⁰, F. Fan⁷, A. Fantoni⁵², M. Fasel⁹⁸, P. Fedichio³⁰, A. Feliciello⁶⁰, G. Feofilov¹¹⁴, A. Fernández Téllez⁴⁵, A. Ferrero¹⁴⁰, A. Ferretti²⁴, V.J.G. Feuillard¹⁰⁶, J. Figiel¹¹⁹, V. Filova³⁷, D. Finogeev⁶⁴, F.M. Fionda⁵⁵, G. Fiorenza^{34,108}, F. Flor¹²⁶, A.N. Flores¹²⁰, S. Foertsch⁷³, S. Fokin⁹⁰, E. Fragiaco⁶¹, E. Frajna¹⁴⁷, A. Francisco¹³⁷, U. Fuchs³⁴, N. Funicello²⁹, C. Furget⁸⁰, A. Furs⁶⁴, J.J. Gaardhøje⁹¹, M. Gagliardi²⁴, A.M. Gago¹¹³, A. Gal¹³⁹, C.D. Galvan¹²¹, P. Ganoti⁸⁶, C. Garabatos¹⁰⁹, J.R.A. Garcia⁴⁵, E. Garcia-Solis¹⁰, K. Garg¹¹⁶, C. Gargiulo³⁴, A. Garibli⁸⁹, K. Garner¹⁴⁶, P. Gasik¹⁰⁹, E.F. Gauger¹²⁰, A. Gautam¹²⁸, M.B. Gay Ducati⁷¹, M. Germain¹¹⁶, P. Ghosh¹⁴³, S.K. Ghosh⁴, M. Giacalone²⁵, P. Gianotti⁵², P. Giubellino^{109,60}, P. Giubilato²⁷, A.M.C. Glaenger¹⁴⁰, P. Glässel¹⁰⁶, E. Glimos¹³², D.J.Q. Goh⁸⁴, V. Gonzalez¹⁴⁵, L.H. González-Trueba⁷², S. Gorbunov³⁹, M. Gorgon², L. Görlich¹¹⁹, S. Gotovac³⁵, V. Grabski⁷², L.K. Graczykowski¹⁴⁴, L. Greiner⁸¹, A. Grelli⁶³, C. Grigoras³⁴, V. Grigoriev⁹⁵, S. Grigoryan^{76,1}, F. Grosa^{34,60}, J.F. Grosse-Oetringhaus³⁴, R. Grosso¹⁰⁹, D. Grund³⁷, G.G. Guardiani¹²³, R. Guernane⁸⁰, M. Guilbaud¹¹⁶, K. Gulbrandsen⁹¹, T. Gunji¹³⁴, W. Guo⁷, A. Gupta¹⁰³, R. Gupta¹⁰³, S.P. Guzman⁴⁵, L. Gyulai¹⁴⁷, M.K. Habib¹⁰⁹, C. Hadjidakis⁷⁹, H. Hamagaki⁸⁴, M. Hamid⁷, R. Hannigan¹²⁰, M.R. Haque¹⁴⁴, A. Harlanderova¹⁰⁹, J.W. Harris¹⁴⁸, A. Harton¹⁰, J.A. Hasenbichler³⁴, H. Hassan⁹⁸, D. Hatzifotiadou⁵⁴, P. Hauer⁴³, L.B. Havener¹⁴⁸, S.T. Heckel¹⁰⁷, E. Hellbär¹⁰⁹, H. Helstrup³⁶, T. Herman³⁷, E.G. Hernandez⁴⁵, G. Herrera Corral⁹, F. Herrmann¹⁴⁶, K.F. Hetland³⁶, H. Hillemanns³⁴, C. Hills¹²⁹, B. Hippolyte¹³⁹, B. Hofman⁶³, B. Hohlweger⁹², J. Honermann¹⁴⁶, G.H. Hong¹⁴⁹, D. Horak³⁷, S. Hornung¹⁰⁹, A. Horzyk², R. Hosokawa¹⁵, Y. Hou⁷, P. Hristov³⁴, C. Hughes¹³², P. Huhn⁶⁹, L.M. Huhta¹²⁷, C.V. Hulse⁷⁹, T.J. Humanic⁹⁹, H. Hushnud¹¹¹, L.A. Husova¹⁴⁶,

A. Hutson¹²⁶, J.P. Iddon^{34,129}, R. Ilkaev¹¹⁰, H. Ilyas¹⁴, M. Inaba¹³⁵, G.M. Innocenti³⁴, M. Ippolitov⁹⁰, A. Isakov⁹⁷, T. Isidori¹²⁸, M.S. Islam¹¹¹, M. Ivanov¹⁰⁹, V. Ivanov¹⁰⁰, V. Izucheev⁹³, M. Jablonski², B. Jacak⁸¹, N. Jacazio³⁴, P.M. Jacobs⁸¹, S. Jadlovska¹¹⁸, J. Jadlovsky¹¹⁸, S. Jaelani⁶³, C. Jahnke^{123,122}, M.J. Jakubowska¹⁴⁴, A. Jalotra¹⁰³, M.A. Janik¹⁴⁴, T. Janson⁷⁵, M. Jercic¹⁰¹, O. Jevons¹¹², A.A.P. Jimenez⁷⁰, F. Jonas^{98,146}, P.G. Jones¹¹², J.M. Jowett^{34,109}, J. Jung⁶⁹, M. Jung⁶⁹, A. Junique³⁴, A. Jusko¹¹², M.J. Kabus¹⁴⁴, J. Kaewjai¹¹⁷, P. Kalinak⁶⁵, A.S. Kalteyer¹⁰⁹, A. Kalweit³⁴, V. Kaplin⁹⁵, A. Karasu Uysal⁷⁸, D. Karatovic¹⁰¹, O. Karavichev⁶⁴, T. Karavicheva⁶⁴, P. Karczmarczyk¹⁴⁴, E. Karpechev⁶⁴, V. Kashyap⁸⁸, A. Kazantsev⁹⁰, U. Keschull⁷⁵, R. Keidel⁴⁷, D.L.D. Keijdener⁶³, M. Keil³⁴, B. Ketzer⁴³, Z. Khabanova⁹², A.M. Khan⁷, S. Khan¹⁶, A. Khanzadeev¹⁰⁰, Y. Kharlov^{93,83}, A. Khatun¹⁶, A. Khuntia¹¹⁹, B. Kileng³⁶, B. Kim^{17,62}, C. Kim¹⁷, D.J. Kim¹²⁷, E.J. Kim⁷⁴, J. Kim¹⁴⁹, J.S. Kim⁴¹, J. Kim¹⁰⁶, J. Kim⁷⁴, M. Kim¹⁰⁶, S. Kim¹⁸, T. Kim¹⁴⁹, S. Kirsch⁶⁹, I. Kisel³⁹, S. Kiselev⁹⁴, A. Kisiel¹⁴⁴, J.P. Kitowski², J.L. Klay⁶, J. Klein³⁴, S. Klein⁸¹, C. Klein-Bösing¹⁴⁶, M. Kleiner⁶⁹, T. Klemenz¹⁰⁷, A. Kluge³⁴, A.G. Knospe¹²⁶, C. Kobdaj¹¹⁷, T. Kollegger¹⁰⁹, A. Kondratyev⁷⁶, N. Kondratyeva⁹⁵, E. Kondratyuk⁹³, J. König⁶⁹, S.A. Königstorfer¹⁰⁷, P.J. Konopka³⁴, G. Kornakov¹⁴⁴, S.D. Koryciak², A. Kotliarov⁹⁷, O. Kovalenko⁸⁷, V. Kovalenko¹¹⁴, M. Kowalski¹¹⁹, I. Králik⁶⁵, A. Kravčáková³⁸, L. Kreis¹⁰⁹, M. Krivda^{112,65}, F. Krizek⁹⁷, K. Krizkova Gajdosova³⁷, M. Kroesen¹⁰⁶, M. Krüger⁶⁹, D.M. Krupova³⁷, E. Kryshen¹⁰⁰, M. Krzewicki³⁹, V. Kučera³⁴, C. Kuhn¹³⁹, P.G. Kuijper⁹², T. Kumaoka¹³⁵, D. Kumar¹⁴³, L. Kumar¹⁰², N. Kumar¹⁰², S. Kundu³⁴, P. Kurashvili⁸⁷, A. Kurepin⁶⁴, A.B. Kurepin⁶⁴, A. Kuryakin¹¹⁰, S. Kushpil⁹⁷, J. Kvapil¹¹², M.J. Kweon⁶², J.Y. Kwon⁶², Y. Kwon¹⁴⁹, S.L. La Pointe³⁹, P. La Rocca²⁶, Y.S. Lai⁸¹, A. Lakrathok¹¹⁷, M. Lamanna³⁴, R. Langoy¹³¹, K. Lapidus³⁴, P. Larionov^{34,52}, E. Laudi³⁴, L. Lautner^{34,107}, R. Lavicka^{115,37}, T. Lazareva¹¹⁴, R. Lea^{142,23,58}, J. Lehrbach³⁹, R.C. Lemmon⁹⁶, I. León Monzón¹²¹, E.D. Lesser¹⁹, M. Lettrich^{34,107}, P. Lévai¹⁴⁷, X. Li¹¹, X.L. Li⁷, J. Lien¹³¹, R. Lietava¹¹², B. Lim¹⁷, S.H. Lim¹⁷, V. Lindenstruth³⁹, A. Lindner⁴⁸, C. Lippmann¹⁰⁹, A. Liu¹⁹, D.H. Liu⁷, J. Liu¹²⁹, I.M. Lofnes²¹, V. Loginov⁹⁵, C. Loizides⁹⁸, P. Loncar³⁵, J.A. Lopez¹⁰⁶, X. Lopez¹³⁷, E. López Torres⁸, J.R. Luhder¹⁴⁶, M. Lunardon²⁷, G. Luparello⁶¹, Y.G. Ma⁴⁰, A. Maevskaya⁶⁴, M. Mager³⁴, T. Mahmoud⁴³, A. Maire¹³⁹, M. Malaev¹⁰⁰, N.M. Malik¹⁰³, Q.W. Malik²⁰, S.K. Malik¹⁰³, L. Malinina^{14,76}, D. Mal'Kevich⁹⁴, D. Mallick⁸⁸, N. Mallick⁵⁰, G. Mandaglio^{32,56}, V. Manko⁹⁰, F. Manso¹³⁷, V. Manzari⁵³, Y. Mao⁷, G.V. Margagliotti²³, A. Margotti⁵⁴, A. Marín¹⁰⁹, C. Markert¹²⁰, M. Marquard⁶⁹, N.A. Martin¹⁰⁶, P. Martinengo³⁴, J.L. Martinez¹²⁶, M.I. Martínez⁴⁵, G. Martínez García¹¹⁶, S. Masciocchi¹⁰⁹, M. Maserà²⁴, A. Masoni⁵⁵, L. Massacrier⁷⁹, A. Mastroserio^{141,53}, A.M. Mathis¹⁰⁷, O. Matonoha⁸², P.F.T. Matuoka¹²², A. Matyja¹¹⁹, C. Mayer¹¹⁹, A.L. Mazuecos³⁴, F. Mazzaschi²⁴, M. Mazzilli³⁴, M.A. Mazzoni^{1,59}, J.E. Mdhluli¹³³, A.F. Mechler⁶⁹, Y. Melikyan⁶⁴, A. Menchaca-Rocha⁷², E. Meninno^{115,29}, A.S. Menon¹²⁶, M. Meres¹³, S. Mhlanga^{125,73}, Y. Miake¹³⁵, L. Micheletti⁶⁰, L.C. Migliorin¹³⁸, D.L. Mihaylov¹⁰⁷, K. Mikhaylov^{76,94}, A.N. Mishra¹⁴⁷, D. Miśkowiec¹⁰⁹, A. Modak⁴, A.P. Mohanty⁶³, B. Mohanty⁸⁸, M. Mohisin Khan¹⁶, M.A. Molander⁴⁴, Z. Moravcova⁹¹, C. Mordasini¹⁰⁷, D.A. Moreira De Godoy¹⁴⁶, I. Morozov⁶⁴, A. Morsch³⁴, T. Mrnjavac³⁴, V. Muccifora⁵², E. Mudnic³⁵, D. Mühlheim¹⁴⁶, S. Muhuri¹⁴³, J.D. Mulligan⁸¹, A. Mulliri²², M.G. Munhoz¹²², R.H. Munzer⁶⁹, H. Murakami¹³⁴, S. Murray¹²⁵, L. Musa³⁴, J. Musinsky⁶⁵, J.W. Myrcha¹⁴⁴, B. Naik¹³³, R. Nair⁸⁷, B.K. Nandi⁴⁹, R. Nania⁵⁴, E. Nappi⁵³, A.F. Nassirpour⁸², A. Nath¹⁰⁶, C. Nattrass¹³², A. Neagu²⁰, A. Negru¹³⁶, L. Nellen⁷⁰, S.V. Nesbo³⁶, G. Neskovic³⁹, D. Nesterov¹¹⁴, B.S. Nielsen⁹¹, S. Nikolaev⁹⁰, S. Nikulin⁹⁰, V. Nikulin¹⁰⁰, F. Noferini⁵⁴, S. Noh¹², P. Nomokonov⁷⁶, J. Norman¹²⁹, N. Novitzky¹³⁵, P. Nowakowski¹⁴⁴, A. Nyman⁹⁰, J. Nystrand²¹, M. Ogino⁸⁴, A. Ohlson⁸², V.A. Okorokov⁹⁵, J. Oleniacz¹⁴⁴, A.C. Oliveira Da Silva¹³², M.H. Oliver¹⁴⁸, A. Onnerstad¹²⁷, C. Oppedisano⁶⁰, A. Ortiz Velasquez⁷⁰, T. Osako⁴⁶, A. Oskarsson⁸², J. Otwinowski¹¹⁹, M. Oya⁴⁶, K. Oyama⁸⁴, Y. Pachmayer¹⁰⁶, S. Padhan⁴⁹, D. Pagano^{142,58}, G. Paic⁷⁰, A. Palasciano⁵³, J. Pan¹⁴⁵, S. Panebianco¹⁴⁰, J. Park⁶², J.E. Parkkila¹²⁷, S.P. Pathak¹²⁶, R.N. Patra^{103,34}, B. Paul²², H. Pei⁷, T. Peitzmann⁶³, X. Peng⁷, L.G. Pereira⁷¹, H. Pereira Da Costa¹⁴⁰, D. Peresunko^{90,83}, G.M. Perez⁸, S. Perrin¹⁴⁰, Y. Pestov⁵, V. Petráček³⁷, M. Petrovici⁴⁸, R.P. Pezzi^{116,71}, S. Piano⁶¹, M. Pikna¹³, P. Pillot¹¹⁶, O. Pinazza^{54,34}, L. Pinsky¹²⁶, C. Pinto²⁶, S. Pisano⁵², M. Płoskoń⁸¹, M. Planinic¹⁰¹, F. Pliquett⁶⁹, M.G. Poghosyan⁹⁸, B. Polichtchouk⁹³, S. Politano³⁰, N. Poljak¹⁰¹, A. Pop⁴⁸, S. Porteboeuf-Houssais¹³⁷, J. Porter⁸¹, V. Pozdniakov⁷⁶, S.K. Prasad⁴, R. Preghenella⁵⁴, F. Prino⁶⁰, C.A. Pruneau¹⁴⁵, I. Pshenichnov⁶⁴, M. Puccio³⁴, S. Qiu⁹², L. Quaglia²⁴, R.E. Quishpe¹²⁶, S. Ragoni¹¹², A. Rakotozafindrabe¹⁴⁰, L. Ramello³¹, F. Rami¹³⁹, S.A.R. Ramirez⁴⁵, A.G.T. Ramos³³, T.A. Rancien⁸⁰, R. Raniwala¹⁰⁴, S. Raniwala¹⁰⁴, S.S. Räsänen⁴⁴, R. Rath⁵⁰, I. Ravasenga⁹², K.F. Read^{98,132}, A.R. Redelbach³⁹, K. Redlich^{16,87}, A. Rehman²¹, P. Reichelt⁶⁹, F. Reidt³⁴, H.A. Reme-ness³⁶, Z. Rescakova³⁸, K. Reygers¹⁰⁶, A. Riabov¹⁰⁰, V. Riabov¹⁰⁰, T. Richert⁸², M. Richter²⁰, W. Riegler³⁴, F. Riggi²⁶, C. Ristea⁶⁸, M. Rodríguez Cahuantzi⁴⁵, K. Røed²⁰, R. Rogalev⁹³, E. Rogochaya⁷⁶, T.S. Rogoschinski⁶⁹, D. Rohr³⁴, D. Röhrich²¹, P.F. Rojas⁴⁵, S. Rojas Torres³⁷, P.S. Rokita¹⁴⁴, F. Ronchetti⁵², A. Rosano^{32,56}, E.D. Rosas⁷⁰, A. Rossi⁵⁷, A. Roy⁵⁰, P. Roy¹¹¹, S. Roy⁴⁹, N. Rubini²⁵, O.V. Rueda⁸², D. Ruggiano¹⁴⁴, R. Rui²³, B. Rumyantsev⁷⁶, P.G. Russek², R. Russo⁹², A. Rustamov⁸⁹,

E. Ryabinkin⁹⁰, Y. Ryabov¹⁰⁰, A. Rybicki¹¹⁹, H. Rytkonen¹²⁷, W. Rzesza¹⁴⁴, O.A.M. Saarimaki⁴⁴, R. Sadek¹¹⁶, S. Sadovsky⁹³, J. Saetre²¹, K. Šafařík³⁷, S.K. Saha¹⁴³, S. Saha⁸⁸, B. Sahoo⁴⁹, P. Sahoo⁴⁹, R. Sahoo⁵⁰, S. Sahoo⁶⁶, D. Sahu⁵⁰, P.K. Sahu⁶⁶, J. Saini¹⁴³, S. Sakai¹³⁵, M.P. Salvan¹⁰⁹, S. Sambyal¹⁰³, V. Samsonov^{I,100,95}, T.B. Saramela¹²², D. Sarkar¹⁴⁵, N. Sarkar¹⁴³, P. Sarma⁴², V.M. Sarti¹⁰⁷, M.H.P. Sas¹⁴⁸, J. Schambach⁹⁸, H.S. Scheid⁶⁹, C. Schiaua⁴⁸, R. Schicker¹⁰⁶, A. Schmah¹⁰⁶, C. Schmidt¹⁰⁹, H.R. Schmidt¹⁰⁵, M.O. Schmidt^{34,106}, M. Schmidt¹⁰⁵, N.V. Schmidt^{98,69}, A.R. Schmier¹³², R. Schotter¹³⁹, J. Schukraft³⁴, K. Schwarz¹⁰⁹, K. Schweda¹⁰⁹, G. Scioli²⁵, E. Scomparin⁶⁰, J.E. Seger¹⁵, Y. Sekiguchi¹³⁴, D. Sekihata¹³⁴, I. Selyuzhenkov^{109,95}, S. Senyukov¹³⁹, J.J. Seo⁶², D. Serebryakov⁶⁴, L. Šerkšnyte¹⁰⁷, A. Sevcenco⁶⁸, T.J. Shaba⁷³, A. Shabanov⁶⁴, A. Shabetai¹¹⁶, R. Shahoyan³⁴, W. Shaikh¹¹¹, A. Shangaraev⁹³, A. Sharma¹⁰², H. Sharma¹¹⁹, M. Sharma¹⁰³, N. Sharma¹⁰², S. Sharma¹⁰³, U. Sharma¹⁰³, A. Shatat⁷⁹, O. Sheibani¹²⁶, K. Shigaki⁴⁶, M. Shimomura⁸⁵, S. Shirinkin⁹⁴, Q. Shou⁴⁰, Y. Sibiriak⁹⁰, S. Siddhanta⁵⁵, T. Siemiarczuk⁸⁷, T.F. Silva¹²², D. Silvermyr⁸², T. Simantathammakul¹¹⁷, G. Simonetti³⁴, B. Singh¹⁰⁷, R. Singh⁸⁸, R. Singh¹⁰³, R. Singh⁵⁰, V.K. Singh¹⁴³, V. Singhal¹⁴³, T. Sinha¹¹¹, B. Sitar¹³, M. Sitta³¹, T.B. Skaali²⁰, G. Skorodumovs¹⁰⁶, M. Slupecki⁴⁴, N. Smirnov¹⁴⁸, R.J.M. Snellings⁶³, C. Soncco¹¹³, J. Song¹²⁶, A. Songmoolnak¹¹⁷, F. Soramel²⁷, S. Sorensen¹³², I. Sputowska¹¹⁹, J. Stachel¹⁰⁶, I. Stan⁶⁸, P.J. Steffanic¹³², S.F. Stiefelmaier¹⁰⁶, D. Stocco¹¹⁶, I. Storehaug²⁰, M.M. Storetvedt³⁶, P. Stratmann¹⁴⁶, C.P. Stylianidis⁹², A.A.P. Suaide¹²², C. Suire⁷⁹, M. Sukhanov⁶⁴, M. Suljic³⁴, R. Sultanov⁹⁴, V. Sumberia¹⁰³, S. Sumowidagdo⁵¹, S. Swain⁶⁶, A. Szabo¹³, I. Szarka¹³, U. Tabassam¹⁴, S.F. Taghavi¹⁰⁷, G. Taillepied¹³⁷, J. Takahashi¹²³, G.J. Tambave²¹, S. Tang^{137,7}, Z. Tang¹³⁰, J.D. Tapia Takaki^{VII,128}, M. Tarhini¹¹⁶, M.G. Tarzila⁴⁸, A. Tauro³⁴, G. Tejada Muñoz⁴⁵, A. Telesca³⁴, L. Terlizzi²⁴, C. Terrevoli¹²⁶, G. Tersimonov³, S. Thakur¹⁴³, D. Thomas¹²⁰, R. Tieulent¹³⁸, A. Tikhonov⁶⁴, A.R. Timmins¹²⁶, M. Tkacik¹¹⁸, A. Toia⁶⁹, N. Topilskaya⁶⁴, M. Toppi⁵², F. Torres-Acosta¹⁹, T. Tork⁷⁹, A. Trifiró^{32,56}, S. Tripathy^{54,70}, T. Tripathy⁴⁹, S. Trogolo^{34,27}, V. Trubnikov³, W.H. Trzaska¹²⁷, T.P. Trzcinski¹⁴⁴, A. Tumkin¹¹⁰, R. Turrisi⁵⁷, T.S. Tveter²⁰, K. Ullaland²¹, A. Uras¹³⁸, M. Urioni^{58,142}, G.L. Usai²², M. Vala³⁸, N. Valle²⁸, S. Vallero⁶⁰, L.V.R. van Doremalen⁶³, M. van Leeuwen⁹², R.J.G. van Weelden⁹², P. Vande Vyvre³⁴, D. Varga¹⁴⁷, Z. Varga¹⁴⁷, M. Varga-Kofarago¹⁴⁷, M. Vasileiou⁸⁶, A. Vasiliev⁹⁰, O. Vázquez Doce^{52,107}, V. Vechernin¹¹⁴, A. Velure²¹, E. Vercellin²⁴, S. Vergara Limón⁴⁵, L. Vermunt⁶³, R. Vértesi¹⁴⁷, M. Verweij⁶³, L. Vickovic³⁵, Z. Vilakazi¹³³, O. Villalobos Baillie¹¹², G. Vino⁵³, A. Vinogradov⁹⁰, T. Virgili²⁹, V. Vislavicius⁹¹, A. Vodopyanov⁷⁶, B. Volkel^{34,106}, M.A. Völkl¹⁰⁶, K. Voloshin⁹⁴, S.A. Voloshin¹⁴⁵, G. Volpe³³, B. von Haller³⁴, I. Vorobyev¹⁰⁷, N. Vozniuk⁶⁴, J. Vrláková³⁸, B. Wagner²¹, C. Wang⁴⁰, D. Wang⁴⁰, M. Weber¹¹⁵, A. Wegrzynek³⁴, S.C. Wenzel³⁴, J.P. Wessels¹⁴⁶, J. Wiechula⁶⁹, J. Wikne²⁰, G. Wilk⁸⁷, J. Wilkinson¹⁰⁹, G.A. Willems¹⁴⁶, B. Windelband¹⁰⁶, M. Winn¹⁴⁰, W.E. Witt¹³², J.R. Wright¹²⁰, W. Wu⁴⁰, Y. Wu¹³⁰, R. Xu⁷, A.K. Yadav¹⁴³, S. Yalcin⁷⁸, Y. Yamaguchi⁴⁶, K. Yamakawa⁴⁶, S. Yang²¹, S. Yano⁴⁶, Z. Yin⁷, I.-K. Yoo¹⁷, J.H. Yoon⁶², S. Yuan²¹, A. Yuncu¹⁰⁶, V. Zaccolo²³, C. Zampolli³⁴, H.J.C. Zanoli⁶³, N. Zardoshti³⁴, A. Zarochentsev¹¹⁴, P. Závada⁶⁷, N. Zaviyalov¹¹⁰, M. Zhalov¹⁰⁰, B. Zhang⁷, S. Zhang⁴⁰, X. Zhang⁷, Y. Zhang¹³⁰, V. Zhrebchevskii¹¹⁴, Y. Zhi¹¹, N. Zhigareva⁹⁴, D. Zhou⁷, Y. Zhou⁹¹, J. Zhu^{109,7}, Y. Zhu⁷, G. Zinoviev^{1,3}, N. Zurlo^{142,58}

Affiliation Notes

^I Deceased

^{II} Also at: Italian National Agency for New Technologies, Energy and Sustainable Economic Development (ENEA), Bologna, Italy

^{III} Also at: Dipartimento DET del Politecnico di Torino, Turin, Italy

^{IV} Also at: M.V. Lomonosov Moscow State University, D.V. Skobeltsyn Institute of Nuclear, Physics, Moscow, Russia

^V Also at: Department of Applied Physics, Aligarh Muslim University, Aligarh, India

^{VI} Also at: Institute of Theoretical Physics, University of Wrocław, Poland

^{VII} Also at: University of Kansas, Lawrence, Kansas, United States

Collaboration Institutes

¹ A.I. Alikhanyan National Science Laboratory (Yerevan Physics Institute) Foundation, Yerevan, Armenia

² AGH University of Science and Technology, Cracow, Poland

³ Bogolyubov Institute for Theoretical Physics, National Academy of Sciences of Ukraine, Kiev, Ukraine

- ⁴ Bose Institute, Department of Physics and Centre for Astroparticle Physics and Space Science (CAPSS), Kolkata, India
- ⁵ Budker Institute for Nuclear Physics, Novosibirsk, Russia
- ⁶ California Polytechnic State University, San Luis Obispo, California, United States
- ⁷ Central China Normal University, Wuhan, China
- ⁸ Centro de Aplicaciones Tecnológicas y Desarrollo Nuclear (CEADEN), Havana, Cuba
- ⁹ Centro de Investigación y de Estudios Avanzados (CINVESTAV), Mexico City and Mérida, Mexico
- ¹⁰ Chicago State University, Chicago, Illinois, United States
- ¹¹ China Institute of Atomic Energy, Beijing, China
- ¹² Chungbuk National University, Cheongju, Republic of Korea
- ¹³ Comenius University Bratislava, Faculty of Mathematics, Physics and Informatics, Bratislava, Slovakia
- ¹⁴ COMSATS University Islamabad, Islamabad, Pakistan
- ¹⁵ Creighton University, Omaha, Nebraska, United States
- ¹⁶ Department of Physics, Aligarh Muslim University, Aligarh, India
- ¹⁷ Department of Physics, Pusan National University, Pusan, Republic of Korea
- ¹⁸ Department of Physics, Sejong University, Seoul, Republic of Korea
- ¹⁹ Department of Physics, University of California, Berkeley, California, United States
- ²⁰ Department of Physics, University of Oslo, Oslo, Norway
- ²¹ Department of Physics and Technology, University of Bergen, Bergen, Norway
- ²² Dipartimento di Fisica dell'Università and Sezione INFN, Cagliari, Italy
- ²³ Dipartimento di Fisica dell'Università and Sezione INFN, Trieste, Italy
- ²⁴ Dipartimento di Fisica dell'Università and Sezione INFN, Turin, Italy
- ²⁵ Dipartimento di Fisica e Astronomia dell'Università and Sezione INFN, Bologna, Italy
- ²⁶ Dipartimento di Fisica e Astronomia dell'Università and Sezione INFN, Catania, Italy
- ²⁷ Dipartimento di Fisica e Astronomia dell'Università and Sezione INFN, Padova, Italy
- ²⁸ Dipartimento di Fisica e Nucleare e Teorica, Università di Pavia, Pavia, Italy
- ²⁹ Dipartimento di Fisica 'E.R. Caianiello' dell'Università and Gruppo Collegato INFN, Salerno, Italy
- ³⁰ Dipartimento DISAT del Politecnico and Sezione INFN, Turin, Italy
- ³¹ Dipartimento di Scienze e Innovazione Tecnologica dell'Università del Piemonte Orientale and INFN Sezione di Torino, Alessandria, Italy
- ³² Dipartimento di Scienze MIFT, Università di Messina, Messina, Italy
- ³³ Dipartimento Interateneo di Fisica 'M. Merlin' and Sezione INFN, Bari, Italy
- ³⁴ European Organization for Nuclear Research (CERN), Geneva, Switzerland
- ³⁵ Faculty of Electrical Engineering, Mechanical Engineering and Naval Architecture, University of Split, Split, Croatia
- ³⁶ Faculty of Engineering and Science, Western Norway University of Applied Sciences, Bergen, Norway
- ³⁷ Faculty of Nuclear Sciences and Physical Engineering, Czech Technical University in Prague, Prague, Czech Republic
- ³⁸ Faculty of Science, P.J. Šafárik University, Košice, Slovakia
- ³⁹ Frankfurt Institute for Advanced Studies, Johann Wolfgang Goethe-Universität Frankfurt, Frankfurt, Germany
- ⁴⁰ Fudan University, Shanghai, China
- ⁴¹ Gangneung-Wonju National University, Gangneung, Republic of Korea
- ⁴² Gauhati University, Department of Physics, Guwahati, India
- ⁴³ Helmholtz-Institut für Strahlen- und Kernphysik, Rheinische Friedrich-Wilhelms-Universität Bonn, Bonn, Germany
- ⁴⁴ Helsinki Institute of Physics (HIP), Helsinki, Finland
- ⁴⁵ High Energy Physics Group, Universidad Autónoma de Puebla, Puebla, Mexico
- ⁴⁶ Hiroshima University, Hiroshima, Japan
- ⁴⁷ Hochschule Worms, Zentrum für Technologietransfer und Telekommunikation (ZTT), Worms, Germany
- ⁴⁸ Horia Hulubei National Institute of Physics and Nuclear Engineering, Bucharest, Romania
- ⁴⁹ Indian Institute of Technology Bombay (IIT), Mumbai, India
- ⁵⁰ Indian Institute of Technology Indore, Indore, India
- ⁵¹ Indonesian Institute of Sciences, Jakarta, Indonesia
- ⁵² INFN, Laboratori Nazionali di Frascati, Frascati, Italy
- ⁵³ INFN, Sezione di Bari, Bari, Italy
- ⁵⁴ INFN, Sezione di Bologna, Bologna, Italy

- 55 INFN, Sezione di Cagliari, Cagliari, Italy
- 56 INFN, Sezione di Catania, Catania, Italy
- 57 INFN, Sezione di Padova, Padova, Italy
- 58 INFN, Sezione di Pavia, Pavia, Italy
- 59 INFN, Sezione di Roma, Rome, Italy
- 60 INFN, Sezione di Torino, Turin, Italy
- 61 INFN, Sezione di Trieste, Trieste, Italy
- 62 Inha University, Incheon, Republic of Korea
- 63 Institute for Gravitational and Subatomic Physics (GRASP), Utrecht University/Nikhef, Utrecht, Netherlands
- 64 Institute for Nuclear Research, Academy of Sciences, Moscow, Russia
- 65 Institute of Experimental Physics, Slovak Academy of Sciences, Košice, Slovakia
- 66 Institute of Physics, Homi Bhabha National Institute, Bhubaneswar, India
- 67 Institute of Physics of the Czech Academy of Sciences, Prague, Czech Republic
- 68 Institute of Space Science (ISS), Bucharest, Romania
- 69 Institut für Kernphysik, Johann Wolfgang Goethe-Universität Frankfurt, Frankfurt, Germany
- 70 Instituto de Ciencias Nucleares, Universidad Nacional Autónoma de México, Mexico City, Mexico
- 71 Instituto de Física, Universidade Federal do Rio Grande do Sul (UFRGS), Porto Alegre, Brazil
- 72 Instituto de Física, Universidad Nacional Autónoma de México, Mexico City, Mexico
- 73 iThemba LABS, National Research Foundation, Somerset West, South Africa
- 74 Jeonbuk National University, Jeonju, Republic of Korea
- 75 Johann-Wolfgang-Goethe Universität Frankfurt Institut für Informatik, Fachbereich Informatik und Mathematik, Frankfurt, Germany
- 76 Joint Institute for Nuclear Research (JINR), Dubna, Russia
- 77 Korea Institute of Science and Technology Information, Daejeon, Republic of Korea
- 78 KTO Karatay University, Konya, Turkey
- 79 Laboratoire de Physique des 2 Infinis, Irène Joliot-Curie, Orsay, France
- 80 Laboratoire de Physique Subatomique et de Cosmologie, Université Grenoble-Alpes, CNRS-IN2P3, Grenoble, France
- 81 Lawrence Berkeley National Laboratory, Berkeley, California, United States
- 82 Lund University Department of Physics, Division of Particle Physics, Lund, Sweden
- 83 Moscow Institute for Physics and Technology, Moscow, Russia
- 84 Nagasaki Institute of Applied Science, Nagasaki, Japan
- 85 Nara Women's University (NWU), Nara, Japan
- 86 National and Kapodistrian University of Athens, School of Science, Department of Physics, Athens, Greece
- 87 National Centre for Nuclear Research, Warsaw, Poland
- 88 National Institute of Science Education and Research, Homi Bhabha National Institute, Jatni, India
- 89 National Nuclear Research Center, Baku, Azerbaijan
- 90 National Research Centre Kurchatov Institute, Moscow, Russia
- 91 Niels Bohr Institute, University of Copenhagen, Copenhagen, Denmark
- 92 Nikhef, National institute for subatomic physics, Amsterdam, Netherlands
- 93 NRC Kurchatov Institute IHEP, Protvino, Russia
- 94 NRC «Kurchatov» Institute - ITEP, Moscow, Russia
- 95 NRNU Moscow Engineering Physics Institute, Moscow, Russia
- 96 Nuclear Physics Group, STFC Daresbury Laboratory, Daresbury, United Kingdom
- 97 Nuclear Physics Institute of the Czech Academy of Sciences, Řež u Prahy, Czech Republic
- 98 Oak Ridge National Laboratory, Oak Ridge, Tennessee, United States
- 99 Ohio State University, Columbus, Ohio, United States
- 100 Petersburg Nuclear Physics Institute, Gatchina, Russia
- 101 Physics department, Faculty of science, University of Zagreb, Zagreb, Croatia
- 102 Physics Department, Panjab University, Chandigarh, India
- 103 Physics Department, University of Jammu, Jammu, India
- 104 Physics Department, University of Rajasthan, Jaipur, India
- 105 Physikalisches Institut, Eberhard-Karls-Universität Tübingen, Tübingen, Germany
- 106 Physikalisches Institut, Ruprecht-Karls-Universität Heidelberg, Heidelberg, Germany
- 107 Physik Department, Technische Universität München, Munich, Germany
- 108 Politecnico di Bari and Sezione INFN, Bari, Italy

- ¹⁰⁹ Research Division and ExtreMe Matter Institute EMMI, GSI Helmholtzzentrum für Schwerionenforschung GmbH, Darmstadt, Germany
- ¹¹⁰ Russian Federal Nuclear Center (VNIIEF), Sarov, Russia
- ¹¹¹ Saha Institute of Nuclear Physics, Homi Bhabha National Institute, Kolkata, India
- ¹¹² School of Physics and Astronomy, University of Birmingham, Birmingham, United Kingdom
- ¹¹³ Sección Física, Departamento de Ciencias, Pontificia Universidad Católica del Perú, Lima, Peru
- ¹¹⁴ St. Petersburg State University, St. Petersburg, Russia
- ¹¹⁵ Stefan Meyer Institut für Subatomare Physik (SMI), Vienna, Austria
- ¹¹⁶ SUBATECH, IMT Atlantique, Université de Nantes, CNRS-IN2P3, Nantes, France
- ¹¹⁷ Suranaree University of Technology, Nakhon Ratchasima, Thailand
- ¹¹⁸ Technical University of Košice, Košice, Slovakia
- ¹¹⁹ The Henryk Niewodniczanski Institute of Nuclear Physics, Polish Academy of Sciences, Cracow, Poland
- ¹²⁰ The University of Texas at Austin, Austin, Texas, United States
- ¹²¹ Universidad Autónoma de Sinaloa, Culiacán, Mexico
- ¹²² Universidade de São Paulo (USP), São Paulo, Brazil
- ¹²³ Universidade Estadual de Campinas (UNICAMP), Campinas, Brazil
- ¹²⁴ Universidade Federal do ABC, Santo Andre, Brazil
- ¹²⁵ University of Cape Town, Cape Town, South Africa
- ¹²⁶ University of Houston, Houston, Texas, United States
- ¹²⁷ University of Jyväskylä, Jyväskylä, Finland
- ¹²⁸ University of Kansas, Lawrence, Kansas, United States
- ¹²⁹ University of Liverpool, Liverpool, United Kingdom
- ¹³⁰ University of Science and Technology of China, Hefei, China
- ¹³¹ University of South-Eastern Norway, Tonsberg, Norway
- ¹³² University of Tennessee, Knoxville, Tennessee, United States
- ¹³³ University of the Witwatersrand, Johannesburg, South Africa
- ¹³⁴ University of Tokyo, Tokyo, Japan
- ¹³⁵ University of Tsukuba, Tsukuba, Japan
- ¹³⁶ University Politehnica of Bucharest, Bucharest, Romania
- ¹³⁷ Université Clermont Auvergne, CNRS/IN2P3, LPC, Clermont-Ferrand, France
- ¹³⁸ Université de Lyon, CNRS/IN2P3, Institut de Physique des 2 Infinis de Lyon, Lyon, France
- ¹³⁹ Université de Strasbourg, CNRS, IPHC UMR 7178, F-67000 Strasbourg, France, Strasbourg, France
- ¹⁴⁰ Université Paris-Saclay Centre d'Etudes de Saclay (CEA), IRFU, Département de Physique Nucléaire (DPhN), Saclay, France
- ¹⁴¹ Università degli Studi di Foggia, Foggia, Italy
- ¹⁴² Università di Brescia, Brescia, Italy
- ¹⁴³ Variable Energy Cyclotron Centre, Homi Bhabha National Institute, Kolkata, India
- ¹⁴⁴ Warsaw University of Technology, Warsaw, Poland
- ¹⁴⁵ Wayne State University, Detroit, Michigan, United States
- ¹⁴⁶ Westfälische Wilhelms-Universität Münster, Institut für Kernphysik, Münster, Germany
- ¹⁴⁷ Wigner Research Centre for Physics, Budapest, Hungary
- ¹⁴⁸ Yale University, New Haven, Connecticut, United States
- ¹⁴⁹ Yonsei University, Seoul, Republic of Korea